

Wave climate in the Arctic 1992-2014: seasonality and trends

Justin E. Stopa¹, Fabrice Ardhuin¹, and Fanny Girard-Ardhuin¹

¹Univ. Brest, CNRS, IRD, Ifremer, Laboratoire d'Océanographie Physique et Spatiale (LOPS), IUEM, 29280, Brest, France

Correspondence to: Justin E. Stopa (justin.stopa@ifremer.fr)

Abstract. Over the past decade, the diminishing Arctic sea ice has impacted the wave field which ~~is principally dependent~~ depends on the ice-free ~~area-ocean~~ area-ocean and wind. This study characterizes the wave climate in the Arctic ~~using detailed sea state information from a wave hindcast and spanning 1992-2014 from a~~ merged altimeter dataset spanning 1992-2014. The wave model uses winds from the Climate Forecast System Reanalysis and a wave hindcast that uses CFSR winds and ice concentrations ~~derived~~ from satellites as input. The ~~ice concentrations have a grid spacing of 12.5 km, which is sufficiently able to resolve important features in the marginal ice zone. The~~ model performs well, verified by the altimeters, and is relatively consistent for climate studies. The wave seasonality and extremes are linked to the ice coverage, wind strength, and wind direction. ~~This creates creating~~ distinct features in the wind-seas and swells. The ~~increase in wave heights is caused by the loss~~ altimeters and model show that the reduction of sea ice ~~and not the wind verified by the altimeters and model~~ coverage causes the increasing wave heights instead of the wind. However, trends are convoluted by inter-annual climate oscillations like the North Atlantic Oscillation (NAO) and Pacific Decadal Oscillation. ~~The In the~~ Nordic-Greenland Sea is the only region with negative trends in wind speed and wave height and is related to the NAO the NAO is influencing the decreasing wind speeds and wave heights. Swells are becoming more prevalent and wind-sea steepness is declining ~~which make the impact on sea ice uncertain. The~~ satellite data shows the sea ice minimum occurs later in the Fall; the time of year when wind speeds increase. Therefore, it is expected that the sea state will become more active this season. It is inconclusive how important wave-ice processes are within the climate system, but selected events suggest the importance of waves within the marginal ice zone.

1 Introduction

Sea ice ~~moderates the climate; therefore, the declining ice in Arctic Ocean has direct impacts on~~ plays an important role within the climate directly affecting the Earth's albedo, meridional ocean circulation, biologic ecosystems, and human activities. Satellite measurements from the last 30 years ~~reveal the ice has show~~ Arctic ice decreased by 0.45 to 0.51 million km² or -10.2 to -11.4 % per decade (Hartmann et al., 2013; Comiso et al., 2008). This has a dramatic ~~and direct~~ impact on the sea state because there is a larger expanse of ocean available for wave development (Thomson and Rogers, 2014). Ocean waves ~~have important implications in the Arctic because they~~ drive the upper ocean dynamics influencing the rich biological cycle (Tremblay et al., 2008; Popova et al., 2010). Near the Alaska coastline waves are causing erosion (Overeem et al., 2011), and as the ocean opens connecting the Atlantic and Pacific for transportation and commerce, ~~sea state knowledge~~ knowledge of the

1 sea state becomes increasingly important (Stephenson et al., 2011; Jeffries et al., 2013). ~~Therefore it is crucial to improve our~~
2 ~~knowledge of waves in the Arctic Ocean.~~

3 Ice and wave interaction is a highly coupled two-way system. On the one hand, sea ice defines the shape and size of
4 the basin controlling the available ~~sea surface open to the atmosphere for wave growth~~fetch; and on the other hand, waves
5 break-up ice (Marko, 2003). The warming in the past decade ~~has created declining~~decreased sea ice cover (Zhang, 2005;
6 Steele et al., 2008; Screen and Simmonds, 2010; Cavalieri and Parkinson, 2012; Frey et al., 2015). A model simulation of
7 Wang et al. (2015) and data from altimeters ~~of Wang et al. (2015) and Francis et al. (2011) respectively show that with the~~
8 ~~increased in Francis et al. (2011) show that more~~ open water in the Beaufort and Chukchi Seas ~~, wave heights are increasing~~increased
9 wave heights. The objective of this ~~manuscript study~~ is to describe the wave climate in the Arctic Ocean pole ward of 66°N ~~with~~
10 ~~emphasis on resolving wave and ice features at appropriate spatial scales~~. This provides an opportunity to describe the Arctic
11 as a complete system and ~~enables relate~~ our results to ~~be related to~~ existing regional studies in the Nordic Seas (Semedo et al.,
12 2014), the Nordic and Barents Seas (Reistad et al., 2011), and Beaufort-Chukchi Sea (Francis et al., 2011; Wang et al., 2015).

13 Analysis of historical wave observations including in-situ buoy measurements (e.g., Gemmrich et al., 2011), remotely sensed
14 waves from altimeters (e.g., Zieger et al., 2009), observations from voluntary observing ships (e.g., Gulev and Grigorieva,
15 2006), and microseisms (e.g., Husson et al., 2012) give us ~~rich~~useful information about the wave climate. Still, in the Arctic
16 these sources are not entirely satisfactory; ~~therefore, we can use numerical models to provide full space-time details essential for~~
17 ~~a comprehensive description of the wave conditions. WAVEWATCH III. Therefore, we use WAVEWATCH III of~~ (called WW3
18 herein) ~~of Tolman et al. (2013) is a community based spectral wave model that describes wave evolution at the desired spatial~~
19 ~~and temporal resolution and provides the full sea state details through a frequency-direction spectrum. In recent years there~~
20 ~~has been significant improvement to WW3 through the National Partnership Program (NOPP) which developed the physical~~
21 ~~parameterizations important for deep water wave evolution (Tolman and the WAVEWATCH III Development Group, 2014).~~

22 To properly ~~hindcast~~ waves in the Arctic using WW3, it is imperative to use high quality sea ice information and wind in
23 ~~the model~~Tolman and the WAVEWATCH III Development Group (2014) to provide detailed wave conditions. Ice concentra-
24 tions ~~from~~ derived from the Special Sensor Microwave Imager (SSM/I) ~~sufficiently resolve important features in the marginal~~
25 ~~ice zone (MIZ) and have more than two decades of observations. The continuous availability and amount of observations~~
26 ~~make wind reanalysis data the most comprehensive for wave hindcasting. Wave hindcasting using wind reanalysis datasets~~
27 ~~has a long history of successful applications including the National Center for Environmental Prediction (NCEP) Reanalysis~~
28 ~~I (R1) (Wang and Swail, 2001), the European Centre for Medium-Range Weather Forecasts (ECMWF) reanalysis ERA-40~~
29 ~~(Uppala et al., 2005) and ERA-Interim (ERA-Interim) (Dee et al., 2011), and the National Center for Environmental Prediction (NCEP)~~
30 ~~Climate Forecast System reanalysis (CFSR) (Chawla et al., 2013; Rascle and Ardhuin, 2013).~~ To efficiently ~~hindcast in the~~
31 ~~Arctic basin we implement WW3 on a curvilinear grid matching the spatial resolution of ice concentrations at~~ are the longest
32 time series from 1992 to present and have the highest resolution of 12.5 km (Rogers and Orzech, 2013).

33 We ~~hindcast the wave conditions from 1992 to 2014 because this.~~ This time period coincides with available ~~ice concentrations~~
34 ~~from SSM/I and significant wave heights from altimeters starting in 1991. We provide more~~ altimeters so we focus on
35 describing the wave climate for 1992-2014 with both the altimeters and the wave model.

1 The study is organized as follows. We provide background information regarding the model setup, input wind and ice fields,
2 altimeter wave data, and our analysis methodology in section 2. Section 3 focuses on validating our wave modeling efforts
3 using wave heights from altimeters. ~~We then~~ Next we describe the wave climate in section 4, illustrating the seasonality,
4 extreme conditions, and trends of the wave field over the last 23 years. In section 5 we demonstrate the importance of wave-
5 ice interaction through selected wave events. Finally, we discuss the results and give our conclusions in sections 6 and 7
6 respectively.

7 **2 Datasets, Model Implementation and Methodology**

8 The Arctic Ocean is smaller in scale compared to other ~~basins and is~~ oceans; 7000 km at its widest point. The ocean is
9 surrounded by a continental shelf with depths of 300 m. The center of the basin near the North Pole has depths greater than
10 4000 km and is often ice covered. The combination of ice coverage and geography creates the different regional seas shown
11 in Figure 1. ~~The~~ We will distinguish seven sub-regions: 1) Nordic-Greenland Sea, 2) Barents Sea, 3) Kara Sea, 4) Laptev Sea,
12 5) East Siberia Sea, 6) Beaufort-Chukchi Sea, and 7) Baffin Bay ~~are used to generalize the climate~~. The following subsections
13 describe the ~~input and validation datasets~~ ice concentrations, wind reanalysis, satellite altimetry, model setup, and analysis
14 techniques.

15 **2.1 Ice concentration from IFREMER/CERSAT (SSM/I)**

16 Satellite derived ice concentrations are an invaluable data source to observe ice ~~behavior~~ dynamics (e.g., Frey et al., 2015). The
17 Special Sensor Microwave Imager (SSM/I) brightness temperatures accurately estimate sea ice concentration (e.g., Liu and
18 Cavalieri, 1998). The ASI algorithm of Kaleschke et al. (2001) uses a transfer equation that relates the polarization difference
19 to ice concentration ~~as a percentage~~. High frequency channels of SSM/I are used to estimate a daily average on a 12.5 km grid
20 at IFREMER/CERSAT. ~~This resolution enables and describe~~ important spatial features of the MIZ ~~to be resolved~~ (Ezraty
21 et al., 2007). Figure 2 shows the minimum ice extent and total ice area for the period 1992-2014. The time series in the left
22 panel confirms the continual decrease in ice coverage. The minimum sea ice coverage is occurring later in September from
23 1992-2014 with some ~~inter-annual-decadal~~ variability and/or anomalous years of 1997 and 2006. The ~~period 1992-2002 is~~
24 ~~stable followed by an accelerated loss in recent years with the lowest on record~~ sea ice is stable for 1992-2002. Then there is
25 an accelerated reduction in sea ice extent with the ice minimum occurring in 2012. The right panel shows the spatial view of
26 the ice edge minimum from the years 1992-2002, 2002, 2007, and 2012. The East Siberia, Chukchi, and Beaufort Seas have
27 the largest changes in ice cover ~~making them more vulnerable to~~ so we expect increasing waves.

28 **2.2 Reanalysis wind fields**

29 ~~The NCEP CFSR and the ECMWF ERAI winds have been used to drive wave models, and produce high quality wave hindcasts~~
30 ~~(e.g., Chawla et al., 2013; Rasele and Ardhuin, 2013; Stopa and Cheung, 2014; Dee et al., 2014)~~ Wave hindcasts using wind reanalysis
31 datasets have successful applications including the National Center for Environmental Prediction (NCEP) the Climate Forecast

[System reanalysis \(CFSR\) \(Chawla et al., 2013; Raschle and Ardhuin, 2013; Stopa and Cheung, 2014\)](#). The important advancements of CFSR with respect to ~~its~~ predecessors Reanalysis I and II consist of coupling between the ocean, atmosphere, land surface, and sea ice model, assimilation of satellite radiances, and increased horizontal and vertical resolution in the atmospheric model (Saha et al., 2010, 2014). The atmospheric model has a resolution of approximately 0.3° (37 km) (~~v2 has 0.2° 23 km~~) and assimilates data in three dimensions. ~~CFSR is available hourly and winds~~ Wind speeds at 10 m elevation (U10) are ~~used to drive the wave model. The ECMWF ERA-Interim (ERA-Interim) performs well available hourly. In addition, the wave reanalysis of the European Centre for Medium-Range Weather Forecasts (ECMWF) ERA-Interim (ERA-Interim), which couples the atmosphere and wave model and assimilates altimeter wave data, has improved performance~~ over its predecessor ERA-40 ~~with improved~~ (Dee et al., 2011). ERA-Interim has a spatial resolution of 0.7° ~~at with wind every 6 hour intervals~~ hours. The wave reanalysis couples the wave and atmosphere models while assimilating wave data from altimeters (Dee et al., 2011). The dataset is consistent in time and does not have the same discontinuous features as CFSR; but, it is not able to resolve the upper percentiles (Stopa and Cheung, 2014).

It is not evident whether CFSR or ERA-Interim is better suited to drive a wave model in the Arctic. Therefore a concurrent hindcast from 2010-2014 is used to assess the wind forcing differences on the wave field. Appendix A gives a detailed description of the results ~~and herewe summarize~~ summarized here. The largest differences are in the upper percentiles and ERA-Interim significantly underestimates the extreme wave heights. In short, the model errors mirror those of the global basin (Stopa and Cheung, 2014). Due to the importance of resolving the extremes, we use CFSR to re-create the waves from 1992-2014.

2.3 Significant wave heights from altimeters

~~Wave data from altimeters are essential observations for validation and observation. Satellite altimeters provide an extensive source of wave information and have observations every 5.5 km for the hindcast duration~~ Altimeter data has provided an ample source of global wave observations and aided in the development and evaluation of spectral wave models (e.g., Chen et al., 2002; Ardhuin et al., 2002). Significant wave heights (H_s) are measured from active microwave sensors typically in the Ku or Ka bands under all atmospheric conditions. Once the data is quality controlled and sensor biases are removed, H_s errors are comparable to buoy measurements (Zieger et al., 2009; Sepulveda et al., 2015). We use the merged and calibrated dataset of Queffelec and Croize-Fillon (2015). The reprocessed wave measurements from European Remote Sensing Satellites 1 and 2 (ERS1, ERS2), Environmental Satellite (ENVISAT), Geosat Follow-On, CRYOSAT2, and Altika SARAL are used throughout this study. The northern latitude limit is 81.4°N for Geosat Follow-On, 82°N for ERS1, ERS2, ENVISAT, and SARAL, and 88°N for CRYOSAT2. The repeat track cycle is 17 days for Geosat Follow-On, 35 days for ERS1, ERS2, ENVISAT, and SARAL, and 369 days for CRYOSAT2. [The merged dataset spans the duration of the hindcast \(1992-2014\).](#)

2.4 WAVEWATCH III Model Implementation and Wave-ice Dissipation

~~Wave data is generated using the~~ WAVEWATCH III of Tolman et al. (2013) is a community based spectral wave model, WW3 version 5.08 (Tolman and the WAVEWATCH III Development Group, 2014). WW3 evolves the wave action equation in space and time, with discretized wave numbers and directions. Conservative wave processes, represented by the local rate of change

and spatial and spectral transport terms are balanced by the non-conservative sources and sinks. ~~A-We implement version 5.08 of WW3, on a curvilinear grid matching the spatial resolution of ice concentrations at 12.5 km. The curvilinear grid is well suited to model waves near the Poles since the geographic distance between nodes is equal making the computation more efficient (Rogers and Orzech, 2013). The spectra are composed of 24 directions and 32 frequencies exponentially spaced from 0.037 to 0.7 Hz at a relative increment of 1.1. The reanalysis winds are linearly interpolated to the wave model grid.~~ We use WW3's third order the Ultimate Quickest scheme of Tolman (2002) with the garden sprinkler correction. Global 0.5° resolution hindcast of Rascle and Ardhuin (2013) provides the spectral boundary conditions along 66°N. ~~The spatial grid matches the ice resolution of 12.5 km and the spectra are composed of 24 directions and 32 frequencies exponentially spaced from 0.037 to 0.7 Hz at a relative increment of 1.1.~~

The source terms of Ardhuin et al. (2010) describes the wave physics which performs well in terms of H_s , average wave periods, and partitioned wave quantities (Stopa et al., 2015). The wind-wave growth parameter β_{max} is set to 1.25 and otherwise we use the same settings as Rascle and Ardhuin (2013). Due to the importance of wave-ice interactions, a new source term is developed and implemented in WW3 to describe wave dissipation under ice. The dissipation is modeled by a laminar to turbulent boundary layer based on a critical Reynolds number computed from the orbital wave velocity. This parameterization was calibrated using Wadhams and Doble (2009) dataset but still remains somewhat poorly constrained. A full description of the formulation is given in Appendix B.

2.5 Wave parameters and analysis techniques

The wave climate is described using the total significant wave height (H_s) defined as $H_s = 4\sqrt{m_0}$ where m_0 is the zeroth moment ($p=0$) of the spectrum ~~, average ($E(f)$) ($m_p = \int_0^\infty (2\pi f)^p E(f) df$), mean~~ wave period ($T_{m02} = \sqrt{m_0/m_2}$), and average direction (θ_m). ~~The mean wave period has reduced variability compared to other wave period definitions (i.e. peak period or $\sqrt{m-1/m_0}$) since it is calculated from the second moment of the wave spectrum.~~ Swells characterized by longer wavelengths propagate considerable distances under sea ice while high frequency waves are scattered and dissipated near the ice edge (Kohout et al., 2014; Li et al., 2015; Ardhuin et al., 2015). Therefore the ~~wind-waves-wind-seas~~ (H_{sw} , θ_{mw}) and swells (H_{ss} , θ_{ms}) are analyzed separately by partitioning wave spectra using the Hanson and Phillips (2001) method. According to Pierson and Moskowitz (1964) the sea state can be classified as ~~wind-sea-wind-sea~~ when the wave age (WA) or ratio of peak phase speed C_p to wind speed, $WA = C_p/U_{10} < 1.2$ and swell when $WA > 1.2$. Semedo et al. (2011) and Semedo et al. (2014) demonstrated the practicality of this classification through the probability of having a swell dominated wave field (swell persistence): $P_s = P(C_p/U_{10} > 1.2) = N_s/N_{total}$ where N_s is the number of swell dominated events and N_{total} is the total number of events.

In seas with varying ice cover, the method to describe wave statistics ~~becomes increasingly is~~ important (Tuomi et al., 2011). We base our statistics on ice free conditions (ice concentration <15%), but other statistics can be inter-related through the sea ice probability shown in Appendix C. Our results are ~~based-on-calculated using~~ the 3-hour model output for the hindcast duration. H_s percentiles are calculated from the ice-free statistics and the matching H_s index is used to identify corresponding wave periods and directions. A ± 0.2 m bounds of the associated H_s index is used to average the wave periods and directions.

2 This approach gives a more accurate physical description of the events (Anderson et al., 2015). We compute ~~the rate of change~~
3 ~~trends~~ using Sen's ~~slope method~~ and test for ~~significance using the seasonal statistical significance with the~~ Mann-Kendall test.
4 This method is a non parametric technique and a robust way of computing trends since it can handle missing data and is less
5 influenced by outliers (Mann, 1945; Kendall, 1975; Sen, 1968). ~~The method is generalized to~~ We account for the ~~seasonal~~
6 ~~eye-by seasons using the adaptation of~~ Hirsch et al. (1982) and has been used in wave climatology studies by Wang and Swail
7 (2001), Young et al. (2011), and Stopa and Cheung (2014). We compute trends from monthly statistics and require that the
8 time series ~~must be is~~ ice-free for at least 10 years ~~to reduce spurious features~~.

9 3 Wave hindcast validation

10 Before the wave climate is assessed we validate the ~~model hindcast~~ using the merged altimeter dataset for 1992-2014. Altimeter-
11 model co-locations are found using the nearest neighbor within 6 km and 30 minutes. A running mean of 5 points smooths the
12 satellite tracks to make the spatial and temporal scales comparable. The top 4 panels of Figure 3 show four complementary
13 H_s statistics computed in 25 km bins. There is minimal bias for the majority of the domain; however, some errors exist. In
14 the Baffin Bay and the region north of Svalbard there is an underestimation of 5% and 10% respectively. Otherwise spuri-
15 ous negative biases are located near the coasts. In the Beaufort, Chukchi and Laptev Seas the model overestimates the wave
16 heights by 5-10%. The RMSEs are commonly less than 0.4 m. East of Greenland has the largest RMSE of 0.5 m. This area has
17 considerable ice displacements within one day and the SSM/I daily input might not be able to resolve the rapid change. The
18 ~~Nordic Seas, which are ice free year round, have~~ Nordic-Greenland Sea is mostly ice-free year round and thus has the lowest
19 scatter indices (12%) suggesting the model performs well ~~far from the in the absence of sea~~ ice. In contrast ~~regions with to the~~
20 coastal regions of the Baffin Bay, Kara, Laptev, and Beaufort Seas that have considerable ice variability ~~have and create~~ the
21 largest scatter indices of 30%. The model and altimeters are highly correlated with coefficients larger than 0.95. The lowest
22 correlations occur in the Laptev, East Siberia, and East Beaufort Seas. These regions have small wave heights and result in
23 small biases and RMSEs.

24 The bottom panel of Figure 3 shows the consistency of hindcast using the monthly 95th percentile for each satellite mission.
25 The 95th percentile is a rigorous test because it is difficult to resolve extreme waves. The average and median are verified
26 to have no distinct trends (not shown). There is a slight decreasing trend in recent years but it is inconclusive if this trend
27 will continue and is contrary to the global increase observed by Rascle and Ardhuin (2013) for 2006-2011. There ~~is are~~ annual
28 variations but the hindcast is relatively consistent in time making it applicable for climate studies ~~. No noticeable discontinuities~~
29 ~~exist and the hindcast can be used to adequately describe the wave climate in the Arctic Ocean~~ with no noticeable discontinuous
30 features.

31 4 Wave Climate

32 4.1 Seasonality

33 The Arctic Ocean experiences a dramatic seasonal ~~eye~~change. Daily spatial averages of the seven regions in Figure 1 generalize ~~the~~ sea ice, wind speed, and wave seasonality in Figure 4. Two different classifications are identified by the ~~relative~~
1 ~~change in~~ seasonal ice coverage. The ~~first group has small seasonal variation like the Nordie, Greenland, Nordic-Greenland~~
2 ~~and Barents Seas while large seasonality occurs have small seasonal variation while large seasonal changes occur~~ in the Baffin
3 Bay, Beaufort-Chukchi, East Siberia, Laptev, and Kara Seas. All regions have an ice minimum in early September. The wind
4 forcing follows a sinusoid for all seas except the East Siberia Sea with a maximum in January and minimum in July. ~~In The~~
5 regions with reduced ice cover, like the Nordic-Greenland and Barents ~~Sea~~Seas, the waves mirror the wind. Wave heights in
6 the Baffin Bay and Kara Sea, which remain 10% ice free from November to July, follow the winds and can be described by
7 a sinusoid. ~~The wave height seasonal cycle in In~~ the Beaufort-Chukchi, East Siberia, and Laptev Seas ~~is the wave seasons~~
8 ~~are~~ skewed with an annual maximum in October. The antisymmetric ~~pattern seasonal cycle~~ is created by the increasing wind
9 speeds ~~coupled with partially ice-free seas~~ in September and October ~~and partial exposure to the atmosphere~~. Due to the relative
10 difference between the ice and wind we define the winter season as January-February-March (JFM) and the summer season as
11 August-September-October (ASO).

13 Figure 5 presents the wave conditions for the two ~~extremes~~extreme seasons: JFM and ASO. The sea state is described
14 through the H_s , H_{sw} , H_{ss} , and P_s . In JFM, only the ~~Nordie, Greenland~~Nordic-Greenland, and Barents Seas are ice-free.
15 Waves generated in the North Atlantic propagate into these seas with a sheltering in the Barents Sea. ~~The In JFM, the~~ Nordic-
16 Greenland Sea has the tallest wave heights of the Arctic ~~this time of year. The wind waves. The wind seas~~ follow the driving
17 winds ~~and are~~ characterized by cyclonic (anti-clockwise) circulation, ~~which is~~ a characteristic of the North Atlantic sub-basin
18 (Sterl and Caires, 2005; Semedo et al., 2014). The resulting ~~waves wind-sea wave heights~~ exceed 3.5 m while ~~swells have~~
19 ~~smaller heights the swell wave heights are smaller~~ and travel from the Southwest. ~~Even waves generated in the basin are~~
20 ~~classified as swells The top right panel shows swells persist~~ 70% of the time ~~. This which~~ is consistent with open ocean
21 conditions where ~~there are always wind waves and swells wind-seas and swells are ubiquitous~~ (Chen et al., 2002).

22 In ASO, ice coverage is minimum and waves are generated across the Arctic. The H_s pattern in the Nordic, Greenland, and
23 Barents Seas is similar to JFM with only a reduction in magnitude. The ~~other semi-enclosed~~ seas have smaller H_s than the
24 Nordic-Greenland Sea and ~~have wave heights~~ are commonly less than 1.5 m. There are distinct regional characteristics of the
25 wind-seas and swells. The cyclonic structure ~~in of~~ the wind-seas near Norway in JFM is not clearly visible in ASO. The swell
26 ~~mean wave~~ directions follow the same pattern as JFM in the ~~Greenland, Nordie, Nordic-Greenland~~ and Barents Seas and ~~flow~~
27 ~~propagate~~ from the Atlantic northward into the sea ice. In the Laptev and East Siberia Seas the ~~wind waves wind-seas~~ and
28 swells are directed into the sea ice with an Easterly component. H_{sw} and H_{ss} ~~have~~ local maxima located near (170°E, 77°N)
29 where the Easterly waves are able to sufficiently develop. In the Beaufort Sea the wind-sea and swell ~~mean wave~~ directions flow
30 from the Southeast. In the East Beaufort Sea (135°E, 74°N), there is a subtle anti-cyclonic (clockwise) structure in the wind-
31 seas while the swell ~~mean wave~~ directions are opposite and flow from the West. In the narrow corridor of the Baffin Bay, the

wind-sea and swell mean wave directions are opposite and represent different ~~storm-phases~~. ~~The Greenland, Nordic~~ phases of passing storms. The bottom right panel shows the swell persistence is >85% and exceeds 95% in the Nordic-Greenland, Barents Seas, and Baffin Bay ~~are exposed to~~ due to their exposure to the swells generated in the North Atlantic ~~and thus dominated by swells >85 and exceed 95~~. In the semi-enclosed seas like the Kara, Laptev, East Siberia, Beaufort, and Chukchi there is an equal proportion of wind-waves and swells (40-60%).

3 4.2 Percentiles

H_s percentiles are a useful way to describe the sea state statistical distribution (e.g., Stopa et al., 2013a, b). Figure 6 shows the 50th (median), 95th, and 99th H_s percentiles with matching wave directions and average mean periods. The statistics have a consistent spatial pattern due to the geographic shape of the basin. The most prominent feature is the maximum located in the Nordic-Greenland Sea for all percentiles. Here the median H_s exceeds 2.5 m and corresponding T_{m02} is 6 s. In the rest of the basin the H_s median is commonly 1.5 m with reduction near the coasts. The 95th H_s percentile exceeds 5.5 m with T_{m02} of 8 s in the Nordic-Greenland Sea ~~with a reduction in the Barents Sea~~. In the Laptev, East Siberia, Chukchi, and Beaufort Seas the 95th H_s percentiles are 2.5 m with T_{m02} of 6 s. The H_s and T_{m02} at the 99th percentile exceed 8 m and 9 s in the Nordic-Greenland Sea while in the Laptev, East Siberia, Chukchi, and Beaufort Seas are reduced with 4 m and 6.5 s.

The ~~wave directions~~ corresponding wave directions found by using matching indices of the H_s give an indication of the ~~physical nature of the events~~ supporting the approach of finding the matching indices of the H_s percentiles. ~~The directions of the median are~~ wind-sea and swell events. The median is a mix of numerous wave conditions and thus ~~less representative of physical processes because numerous events affect this regime~~ distinct wind-sea and swell events. In the Beaufort-Chukchi Sea the wave directions of the 50th percentile are focused into the ice pack sea ice while for the 95th and 99th percentiles the wave directions flow from the East parallel to the ice edge. Due to the geometry of the Beaufort-Chukchi Sea, the largest fetch occurs when the wind is parallel to the ice edge. ~~So it is not surprising the extreme waves are directed from the East~~. The wave directions of the 95th and 99th percentiles contain similar patterns as the seasonal components of Figure 5. For example the region near East-Greenland is characterized by waves from the North as seen in the wind-waves wind-seas while the waves offshore of Norway are directed from the South typical of swells in JFM. In the Beaufort, Chukchi, and East Siberia Seas ~~the East waves~~, the waves from the East are common to both the wind-waves and swells in JFM and ASO. ~~The percentiles of the semi-enclosed seas have similar magnitude as the Gulf of Mexico (Stopa et al., 2013a)~~.

24 4.3 Trends

With the loss of sea ice ~~it is expected that~~, wave heights are increasing expected to increase. Figure 7 shows Sen's slope computed from monthly averaged quantities with the seasonal Mann-Kendal test for ice coverage and H_s from altimeters and the model. ~~Trends are computed from the monthly averaged quantities with removal of the seasonal cycle~~. The top left panel displays the trend of the SSM/I ice concentrations in number of days per year that are ice-free (i.e. concentration <15%). Most of the ice covered areas are statistically significant and are ice-free 2 additional days each year. The strongest trends are located

30 in the Barents and Kara Seas with 8 more ice-free days per year. ~~Only~~ The isolated regions near Svalbard, Greenland, and the
31 Amundsen Gulf have increasing ice coverage.

32 Most of the basin has increasing wave heights shown by the altimeters and wave model in the top right and bottom panels.
33 The bottom panels show that the co-located H_s trends from the altimeters and the model agree, despite the stronger trends in the
34 altimeters. However, the altimeter confidence interval encompasses the model results so statistically they are equivalent. This is
1 an verification that the CFSR forcing is homogeneous throughout this time period. Discrete satellite passes do not capture the
2 complete space-time history causing spurious trends especially near the MIZ in the East Siberia and Beaufort Seas. The trends
3 computed from the continuous hindcast in the top right panel ~~shows~~ show a spatially consistent pattern. The ice variability is
4 expected to cause the discrepancies in the East Siberia and Beaufort-Chukchi Seas that exist comparing ~~top panel~~ the top and
5 bottom panels. The Nordic-Greenland Sea ~~in is~~ is the only region with a consistent statistically significant decreasing trend shown
6 in the top right panel. In the Beaufort-Chukchi Sea, our rates of 1.5 cm/year are in agreement with Francis et al. (2011) who
7 estimated a trend of 2 cm/year. Wang et al. (2015) estimated trends on the order of 40 cm computed by the difference between
8 1970-1991 and 1992-2013. Assuming a linear rate spanning the 23 year period equates to a 35 cm increase. Some extreme
9 trends greater 4 cm/year exist in the Baffin Bay and Laptev Sea and are significant using the merged altimeters. These rates are
10 ~~very~~ large compared to the global calculations of Young et al. (2011), who estimated the largest trends to be 2 cm/year.

11 Figure 8 shows the ~~trends from other parameters using monthly averages. In this case the results~~ Sen's slope computed
12 from other monthly averaged parameters. The rates are presented as percentages relative to the mean to allow comparison. The
13 trends in U10 are calculated using the entire dataset independent of ice cover; otherwise all other variables are computed from
14 ice-free statistics. The decreasing U10 trend in the ~~Nordic~~ Nordic-Greenland Sea is significant and is consistent with the H_s
15 trend. Across most of the sea ice, U10 is decreasing especially in the Beaufort Sea. Some regions have weak increasing trends
16 of 0.25% per year. Wind speeds in the Baffin Bay are increasing creating taller wave heights.

17 The ~~trends in~~ $Tm02$ trends follow the same pattern as the wave heights in Figure 7 and with an increase of 2% (2-3 cs)
18 per year. The ~~trends in~~ H_{sw} and H_{ss} heights trends have similar spatial patterns as H_s . However, H_{ss} is increasing at a faster
19 rate compared to H_{sw} in the Beaufort, East Siberia, Laptev, and Kara Seas. This is directly related to the higher occurrence
20 of swells (i.e. WA is increasing). The decrease in H_{ss} in the Nordic Sea has less statistically significant points suggesting
21 changes in the local winds are causing the trends. The bottom-center panel displays the ~~wave~~ wind-sea steepness (STw) (ratio
22 of wind-sea wave height versus wavelength) ~~of the wind-sea components. The majority of the basin has a reduction in steepness~~
23 ~~illustrating the wavelengths are increasing faster than the heights.~~ The wave steepness reduces illustrating that the wavelengths
24 become longer than the wave heights are becoming taller. On the other hand, the trends in swell steepness ~~follow~~ have the same
25 pattern as H_s ~~suggesting the meaning the swell~~ wavelengths are changing proportionally to the heights (not shown). Finally the
26 WA is increasing across the entire domain albeit some decreasing regions near the MIZ in the Beaufort Sea, Greenland Sea,
27 and Baffin Bay. Consequently the wave phase speeds are increasing faster than the driving wind fields and swells are becoming
28 more prevalent.

29 Trends often contain a component of variability which may lead to opposite trends in the future. The North Atlantic Oscil-
30 lation (NAO) has a strong influence in the Nordic-Greenland Sea shown by Semedo et al. (2014) and in the Beaufort-Chukchi

Sea, the Pacific Decadal Oscillation (PDO) influences the ice and wind dynamics (Frey et al., 2015). Table 1 presents correlation coefficients between area-averaged monthly time series of sea ice, U10, and H_s and the NAO and PDO indices. ~~The Southern Oscillation Index (SOI) generally had similar correlation coefficients as the PDO but were reduced in strength; so, we only include the PDO here~~ (see Appendix D for spatial distribution). The statistically significant relationship in the wind and wave fields with the NAO is moderate in the the ~~Nordic, Greenland, Nordic-Greenland~~ and Barents Seas. ~~The~~ In these seas, a positive NAO phase equates to increased sea states while a negative phases have reduced sea states. The NAO was positive in the beginning of the time period (1992-1998) and negative towards the end of the hindcast (2006-2012). This creates a negative trend and its positive relationship with the sea states and wind suggests the NAO is causing the negative wind and wave trends observed in Nordic-Greenland and Barents Seas. Table 1 shows the PDO is weakly related in the Beaufort-Chukchi Sea. Higher values are attained by correlating the time series for each point (see Appendix D).

Figure 9 ~~graphically~~ summarizes the regional trends through Sen's slope of the NAO, PDO, ice-free area, U10, and H_s . The NAO and PDO have statistically significant decreasing trends. The NAO is ~~expected to cause~~ influencing the decreasing trend in the Nordic, Greenland, and Barents Seas seen in Figures 7 and 8. The most prominent feature is the increase in ocean area ~~due to the loss of sea ice~~. The H_s trends are not homogeneous showing the regional variability. The largest trends in ocean-area and H_s occur in the Laptev and East Siberia Seas. All seas except the Baffin Bay have stronger trends in the average H_s compared to the 95th percentile suggesting non-uniform changes in the statistical distributions. When the average trend is higher than the 95th percentile it means that moderate events occur more frequent compared to strong events becoming more extreme. In the Baffin Bay the trends in the 95th percentile are larger than the average suggesting the intensification of strong events. The wave trends computed for the co-located altimeters and model show the model underestimates (consistent with Figure 7). The H_s average and 95th percentile ~~often had~~ have larger trends than the results in the global ocean which were typically less than 1% (Young et al., 2011). The trivial U10 trends illustrate the increased sea states are due to ~~ice loss~~ the reduction of ice cover in agreement with Wang et al. (2015).

5 Wave impact on the sea ice

So far, we have seen that ~~the~~ decreasing the sea ice has drastic impacts on the wave climate and has amplified sea states. The waves also impact sea ice and their influence is unknown due to lack of observations and understanding of the wave-ice processes (Squire, 2007; Wadhams and Doble, 2009; Li et al., 2015). Large storms affect the Arctic as demonstrated by Simmonds and Rudeva (2012) and Zhang et al. (2013); however the impacts from waves are less evident. Therefore we qualitatively describe the wave influence on the sea ice with selected events. ~~From the previous analysis, two distinctly different environments emerged. The first is in from the Nordic-Greenland and Beaufort-Chukchi Sea. We chose these regions because their wave environments are different;~~ the Nordic-Greenland Sea ~~and~~ is influenced by swells from the North Atlantic ~~and,~~ the second is Beaufort-Chukchi Sea and the Beaufort-Chukchi Sea is characterized by an equal mix of wind-waves and swells coupled with an extreme change in seasonal ice coverage.

Figure 10 shows the Nordic-Greenland Sea area-averaged ice and sea state conditions for two months in 1992. The 23-year climate average (dashed line) shows the ice cover climatology increases 6% from November through December. The first event, November 23-29, indicates a decrease in ice cover by -3% ~~corresponding to a loss of~~ 60,000 km². This event coincides with H_s , peak periods, and wind speeds exceeding 5 m, 12 s, and 14 m/s respectively. The second event in December has larger wave heights (>6 m), however the ice cover remains the same.

We ~~qualitatively~~ compare and contrast these two events ~~by considering the physical processes of the wind and wave conditions. Figure 11 shows in Figure 11 by showing~~ snapshots of the ~~peak~~ wind speed, wave height, and ~~period for the two selected events. The white and black lines denote wave period. During the November event, the ice edge defined by 15 ice concentration changes considerably before and after the event. During the November event, the (white and black lines). The~~ wind field rotation is cyclonic and centered near Iceland (14°W, 66°N). An anti-cyclonic pattern (6°E, 78°N) adds to the effective fetch. U10 exceeds 20 m/s and H_s exceeds 9 m close proximity to the ice with wave periods ranging 12-15 s. Further into the sea ice only the largest wave periods remain due to the attenuation of the short wavelengths. The wind and wave directions are largely perpendicular to the Greenland ice edge. The largest sea ice changes are located from 70 to 77°N corresponding to the maximum wave energy and wind speed. The bottom panels of Figure 11 show the December storm is located further (7°E, 71°N) from the Greenland ice edge. This ~~creates reduced~~ leads to a reduction of wind speeds (<18 m/s), wave heights (3 m), and periods (12 s) close proximity to the ice edge. ~~There is minimal change to the ice edge during the event and is expected to be.~~ The minimal change in ice coverage is related to the reduced ~~amount of~~ wind and wave energy entering the ice. We do not consider the ice thickness in our analysis; therefore it is not apparent how much ice volume is lost by either event.

Figure 12 shows the ice cover and sea state conditions in the Beaufort-Chukchi Sea in September and October 2006. This time of year the ice increases and advances southward. ~~The September 13-16 and October 9-11 events both have sea ice losses both have changes in sea ice coverage.~~ In the first event the ice coverage reduces by 12% equating to 226,000 km² while in the second event the decrease of 6% equates to 113,000 km². The second event has H_s of 6 m, which is well above the climatology average of 2 m. The sea state is much weaker in the first ~~even~~ event than in the second.

Figure 13 illustrates the corresponding sea state conditions ~~for the events~~. The September case has winds predominately from the South directed into sea ice from the Bering Strait. The wind speeds are ~~expected to be~~ strengthened by the pressure gradient force created by the tall mountain ranges in Alaska and Russia which exceed 2 km in height. The wind speeds, wave heights, and periods reach 18 m/s, 4.5 m and 9 s offshore of the ice. The area of polynya located near (158°W, 77°N) does not change much and is translated towards the Pole. There are significant changes to the ice edge and a large indentation coincides with the maximum wind and wave energy. Besides this isolated section, the rest of the Beaufort ice edge remains the same.

The October event has large wind speeds, wave heights, and wave periods exceeding 24 m/s, 8 m, and 13 s. In fact, this is the strongest event from 23-year hindcast and H_s ~~exceeding~~. The wave heights exceed 8 m and is well above the 99th percentile of Figure 6. The wind field has a cyclonic pattern (~~low-pressure system~~) confirmed to be a Polar Low centered in the Chukchi Sea (162°W, 62°N) and an anti-cyclonic pattern (high-pressure system) centered over the sea ice (132°W, 80°N). The positions of these systems create an extended fetch for wave development because the Eastern winds are directed parallel to the sea ice. Ekman transport could be moving warmer water towards the sea ice. In addition, the extreme wind and waves enhance mixing

32 which could transport warm waters to the ice. As time evolves the systems move further north creating a larger Southerly
33 component in the Eastern portion of the domain where significant impacts ~~are made to the ice edge~~occur in the sea ice.

1 These examples suggest a relationship between the evolution of sea ice and the amount of wind and wave energy ~~that is~~
2 directed into the MIZ. ~~Therefore the orientation of the generating weather systems~~The incident angle of the winds and waves
3 to the sea ice play a critical role on ~~ice evolution~~sea ice; so the location of the storm relative to the ice edge is important.
4 Other physical processes that influence sea ice include temperature change, ocean circulation, and transport due to wind (Frey
5 et al., 2015). ~~And these~~These examples illustrate how waves ~~are expected to~~ impact the sea ice and should be considered as a
6 potential sea ice driver.

7 6 Discussion

8 Coupling between ~~the~~ waves and sea ice is complex (e.g., Squire et al., 1995; Squire, 2007). While the inclusion of the wave-
9 ice dissipation term is a step to incorporate improved wave-ice processes within the wave model, redistribution of the wave
10 energy through scattering must also be considered (Squire et al., 1995). Furthermore, wind-wave generation in partially ice
11 covered waters is expected to be more complex than ~~present as~~parameterized in present wave models (Li et al., 2015). Despite
12 these missing physical processes, the 23-year hindcast presented here performs well offshore of the sea ice as demonstrated by
13 the H_s comparison to the altimeters. ~~The success of the hindcast is reliant on properly describing the sea ice. The SSM/I ice~~
14 ~~concentrations at 12.5 km resolution enables our hindcast to capture important features in the MIZ.~~

15 The seasonal and extreme wave conditions in the Arctic are governed by the sea ice and winds. ~~In most regions the wave~~
16 ~~seasonal variation follows~~The Atlantic side of basin has the most active sea states because it is exposed to the Atlantic and
17 is mostly ice-free year round. Here the wave seasons follow the winds and ~~behaves~~behave like a sinusoid. In semi-enclosed
18 regions like the East-Siberia, Beaufort, and Chukchi Seas the seasonality is skewed with the maximum H_s ~~occurring in October~~
19 ~~which in October and~~ is due to concurrent increasing winds and partially open seas. The isolation of these regions makes them
20 event driven and they have an ~~even~~equal mix of wind-seas and swells. ~~Extreme events~~Here the sea state magnitudes are
21 comparable to those in the Gulf of Mexico (Stopa et al., 2013a) . Extreme events in these seas are limited by the basin's size
22 ~~so the largest events have wave directions and the wave directions are~~ parallel to the ice edge~~in order to attain the largest fetch.~~
23 ~~On the other side of basin, the Nordie-Greenland Sea has the most active sea states within the Arctic because it is exposed~~
24 ~~to the Atlantic and is mostly ice-free year round.~~ Therefore to a leading order the wave behavior is linked to the geography
25 and ice conditions which control the effective fetch for wave development ~~. This supports the non-dimensional fetch scaling of~~
26 ~~Thomson and Rogers (2014) to predict the wave conditions in the Beaufort Sea~~(Thomson and Rogers, 2014; Smith and Thomson, 2016).

27 In the last 23 years, the ~~loss of sea ice but not the driving winds~~reduction of sea ice coverage enabled wave heights to
28 increase ~~in~~as verified by our hindcast and altimeter data sets agreeing with prior studies (Wang et al., 2015; Francis et al.,
29 2011). The sea ice is becoming ice-free for longer durations and the sea ice minimum is occurring later into September as
30 Figure 2-2 suggests. If ice-free conditions persist later into Fall, then seas with skewed seasonal cycles will be sensitive to this
31 change because the wind is stronger~~this season~~. Thus, the Kara, Laptev, East Siberia, Beaufort-Chukchi, and Baffin Bay will be

32 prone to developing larger wave heights in the Fall months when the wind speeds rapidly increase. This has lead Thomson and
33 Rogers (2014) and Thomson and Team (2016) to suggest a positive feedback mechanism linking enhanced wave heights to the
34 larger ocean expanses which cause more ice breakup. However this process is convoluted by the fact that the wave steepness is
35 lessened which reduces the effectiveness of the ice breakup by waves. ~~So even though wave heights are increasing, the waves~~
1 ~~might not be as effective at breaking sea ice because of their reduced steepness.~~

2 The wave response to the changing sea ice through the 21st century is complex with a mix of influences from wind, sea ice,
3 and climate variability (Khon et al., 2014). In ~~our dataset~~ the majority of the Arctic, wave heights are increasing. The only region
4 with decreasing wave heights is in the Nordic-Greenland Sea. In our hindcast time period of 1992-2014, the natural variability
5 of the climate through the NAO ~~, PDO, and SOI~~ and PDO impact the Arctic ~~. The NAO influences the Nordic-Greenland Sea~~
6 ~~and is expected to create the negative trend in U10 and H_s which is unique to the rest of the Arctic that has positive trends~~ sea
7 state. The negative trends observed in the sea state are expected to be caused by the NAO. The PDO influences the Barents and
8 Kara Seas and the monthly correlation coefficients closely aligns with the maximum ice loss ~~trend~~. In the Beaufort-Chukchi
9 Sea the PDO plays a minor role in the wind and wave fields; ~~therefore, the increasing waves are related to declining sea ice.~~
10 ~~When,~~ but this should be monitored when the PDO transitions into a positive phase ~~it might strengthen the Easterly winds,~~
11 ~~which flow parallel to the ice edge, in the Beaufort-Chukchi Sea and result in larger sea states.~~

12 The impact of waves on the sea ice is difficult to determine without detailed knowledge of wave-ice interaction. The evolution
13 of the ice edge seems to ~~response~~ respond to the amount of wind and wave energy near the ice pack as demonstrated ~~by~~
14 ~~computing area-averages of wind and wave quantities~~ in the Nordic-Greenland and Beaufort-Chukchi Seas. ~~This supports the~~
15 ~~idea that the~~ The orientation of the driving wind fields and their incident angles relative to the sea edge is important for sea
16 ice evolution. For example the Great Arctic Cyclone of 2012 persisted for 13 days and had a significant impact on the sea-ice
17 (Simmonds and Rudeva, 2012; Zhang et al., 2013). However, this storm did not produce substantial waves according to our
18 hindcast, due to its passage over ice-covered regions. If the location of the event was positioned more appropriately for wave
19 development, then this ~~type~~ long-lived event could have produced large waves. ~~Therefore if the duration of the storm events~~
20 ~~increases the sea states could achieve full development. The~~ The time duration of the wind and wave influence is less evident
21 in sea ice evolution. For example, the percentage of ice cover remains relatively constant for a 10 day period after the ~~strong~~
22 ~~wave~~ October 2006 event in the Beaufort-Chukchi Sea ~~on October 9, 2006.~~

23 The sea ice variability is influenced by many drivers including atmospheric motion, oceanic motion, air/sea temperatures,
24 and changes in cloud cover (Perovich, 2011). ~~And,~~ waves should also be added to the list ~~as an important sea ice driver.~~

25 7 Conclusion

1 Extending previous studies ~~in~~ of Francis et al. (2011); Wang et al. (2015); Semedo et al. (2014) to the Arctic we produced a
2 23-year wave hindcast from 1992 ~~to~~ through 2014 using CFSR winds and ice concentrations from SSM/I. The combined use
3 of models and satellite observations proves to be a robust way of monitoring and describing the climate. As the Arctic continues
4 to ~~evolve~~ change the results presented here can be used as a basis for future climate ~~conditions~~ studies or projections such as

5 those presented by Khon et al. (2014) or Dobrynin et al. (2012) . Our observed changes in the wave field are expected to be
6 influencing the coastlines, ecosystem, and sea ice melt (e.g., Overeem et al., 2011; Tremblay et al., 2008; Popova et al., 2010; Davis et al.,
7 Since the Arctic is semi-enclosed, the seas-sea states are event driven .The wave field is intertwined with the sea ice coverage
8 and wind conditions where the wind direction defines the effect fetch for wave development. The loss of ice is creating and
9 this creates distinct features in the wind-seas and swells. If the open ocean persists later into the Fall, then the sensitivity of
10 the Arctic sea state and ice conditions will increase since this season has stronger wind speeds. The reduction in ice extent
11 enhanced sea states with influence from large-scale climate oscillationstaller wave heights, longer wavelengths, and more
12 persistent swells. While it is not evident how important wave-ice processes are within the Earth-system, the increasing sea
13 states in the Arctic have-do have critical and direct implications on other important processes. The increasing sea-states are
14 expected to change the air-sea fluxes. The reduced sea ice adjacent to land combined with the increasing sea-states suggests
15 wave-driven coastal hazards and erosion will increase (e.g., Overeem et al., 2011) . Waves induce turbulence and mixing in
16 the upper ocean which are expected to influence the ecosystem (e.g., Tremblay et al., 2008; Popova et al., 2010) . Furthermore
17 higher sea states present larger risks to the growing number of ocean activities and ships operating in the Arctic.-
18 The combination of wave models and satellite data provides sufficient detailed sea state information about the Arctic, and
19 we are essential resources to monitor the changing climatethe environment.

20 Appendix A: The ECMWF Reanalysis Interim and the NCEP Climate Forecast System Reanalysis Arctic

21 Intercomparison 2010-2014

22 Before the 23 year hindcast ~~is implemented,~~ was implemented, we inter-compared two 5-year hindcasts using CFSR and ERAI
23 ~~are inter-compared in order to establish a more suitable~~ winds to establish the better suited wave forcing. ~~Observed-Measured~~
24 wave data is essential for validation and we use ~~buoys and altimeters~~ buoy and altimeter observations. Only a limited number
25 of buoys are available from the National Data Buoy Network (NDBC) in the Chukchi Sea and their locations are shown in
26 Figure 1. ~~These buoys are deployed and collected each season when the ice retreats providing data from July through October~~
27 ~~each year.~~ Only select years and H_s measurements are available from ~~2012 to 2014.~~ The buoys provide essential ground truth
1 ~~for model validation, despite being located~~ July through October (2012-2014) in depths less than 50 m ~~with limited spatial~~
2 ~~coverage.~~

3 Table A1 displays error H_s metric at the buoys. Standard error metrics are used to assess the models including the normalized
4 bias (NBIAS), root mean square error (RMSE), correlation coefficient (R), scatter index (SI), and normalized standard deviation
5 (NSTD) ~~are given below assuming~~ where the x represents the observation and y represents the model, and n is the number of
6 data pairs:

$$7 \quad NBIAS = \left[(\bar{y} - \bar{x}) / \left(\frac{1}{n} \sum_{i=1}^n x_i^2 \right) \right] \times 100 \quad (A1)$$

$$8 \quad RMSE = \sqrt{\frac{1}{n} \sum_{i=1}^n (y_i - x_i)^2} \quad (A2)$$

$$10 \quad R = \sum_{i=1}^n (y_i - \bar{y})(x_i - \bar{x}) / \left[\sqrt{\frac{1}{n} \sum_{i=1}^n (y_i - \bar{y})^2} \sqrt{\frac{1}{n} \sum_{i=1}^n (x_i - \bar{x})^2} \right] \quad (A3)$$

$$12 \quad SI = \left[\sqrt{\frac{1}{n} \sum_{i=1}^n [(y_i - \bar{y}) - (x_i - \bar{x})]^2 / \bar{x}} \right] \times 100 \quad (A4)$$

$$14 \quad NSTD = \left[\sqrt{\frac{1}{n} \sum_{i=1}^n (y_i - \bar{y}) / \sqrt{\frac{1}{n} \sum_{i=1}^n (x_i - \bar{x}) / -1}} \right] \times 100. \quad (A5)$$

16 ~~All buoy have water depths less than 50 m.~~ CFSR Table A1 displays error H_s metric with the NDBC buoys. The CFSR
17 hindcast overestimates the H_s by at least 5% at all locations while ~~ERAI~~ the ERAI hindcast underestimates by 3% (except
18 WMO48213). The RMSEs are commonly 0.25 m with ~~ERAI~~ the ERAI hindcast always having a ~~slightly better match~~ better
19 agreement. The scatter indices and correlation coefficients for the ERAI and CFSR ~~follow the same pattern~~ wave hindcasts are

20 similar at each buoy. The NSTD shows ~~CFSR-the CFSR hindcast~~ has more variability than the observations while ~~ERA1-is-a~~
21 ~~smoother model~~the ERA1 hindcast is smoother. In general both ~~models are comparable with hindcasts are comparable but the~~
22 ~~CFSR hindcast has a positive bias in CFSR and negative bias in ERA1 while the ERA1 hindcast has a negative bias.~~

23 Figure A1 displays two example time series from September 2013 and 2014 at buoys WMO 48213 and 48214 located in
24 the Chukchi Sea. The first example in 2013 shows both models perform reasonably well. ~~ERA1's time series is much smoother~~
25 ~~and creates~~The time series of the ERA1 hindcast is smoother and has a correlation coefficient of 0.89. ~~CFSR-The CFSR~~
26 ~~hindcast~~ is seen to overestimate the events on September 1-3 and 26-28 with differences larger than 0.5 m. For these events
27 ~~ERA1-the ERA1 hindcast~~ follows the same pattern suggesting a systematic error in the forcing wind field or wave physics
28 that are unresolved. The ~~CFSR and ERA1 residuals hindcast residuals (CFSR-buoy and ERA1-buoy hindcasts)~~ are moderately
29 correlated with coefficients of 0.75 showing the forcing wind fields are similar. In September 2014, both ERA1 and CFSR
30 ~~hindcasts~~ are highly correlated to the buoy time series and their residuals are only weakly correlated with a coefficient of 0.37.
31 ~~CFSR-The CFSR hindcast~~ has a consistent positive bias throughout the month, while ~~ERA1-the ERA1 hindcast~~ commonly has
32 errors less than 25 cm. ~~The~~Notice that the peak intensity of wave events is underestimated by ~~ERA1-the ERA1 hindcast~~.

33 ~~The H_s recorded from altimeters provides an extensive dataset for validation. We co-locate~~Figure A2 summarizes the H_s
34 comparison from the altimeter and model ~~by finding the nearest neighbor in space (<6 km) and limit the time difference~~
35 ~~to 30 minutes. A running mean of 5 points is then used to smooth the altimeter tracks in order to make the spatial scales~~
1 ~~comparable between the computational model grid and the altimeter. Figure A2 summarizes the results~~co-locations using the
2 5-year period~~of altimeter-model co-locations~~. The scatterplots from all 2 million data pairs is presented in the top panels. Both
3 datasets are highly correlated with similar SIs of 19% and have RMSEs of 0.4 m. The smooth nature of ~~ERA1-the ERA1~~
4 ~~hindcast~~ creates the negative NSTD of 10% while ~~CFSR-the CFSR hindcast~~ is nearly zero.

5 The largest differences ~~in-between~~ the hindcasts are in the upper wave heights and the bottom panels highlight the differences.
6 Both datasets have similar correlation coefficients of 0.78 and scatter indices of 13%. ~~he-CFSR-The CFSR hindcast~~ has more
7 variability than the observed data creating a NSTD of 20% while ~~ERA1-the ERA1 hindcast~~ matches the variability of the
8 observations much better. From this depiction it is clear that ~~ERA1-the ERA1 hindcast~~ underestimates the largest wave heights.
9 For example the 99th H_s percentile has an average bias of -1.5 m while its -0.1 m for ~~CFSR-the CFSR hindcast~~. These large
10 sea states are important to resolve in practical planning and engineering applications. Therefore caution should be applied
11 when using ~~ERA1-to describe the extreme waves~~extreme waves from a hindcast that uses ERA1 winds as forcing. In our
12 implementation of ~~ERA1-the ERA1 hindcast~~, β_{max} described in Ardhuin et al. (2010) is set to 1.45 and possibly a better match
13 could be achieved by increasing this value. ~~An empirical correction could also be applied similar to Sterl and Caires (2005) with~~
14 ~~ERA-40-~~

15 ~~In the previous comparison it is clear that the upper percentiles are very different. Now, we compare the statistical distributions~~
16 ~~spatially. Figure A3 compare the median~~Figure A3 compares the H_s medians as well as the ~~most extreme wave conditions~~
17 ~~at the 99th percentilepercentiles~~. The top left and center panels display the percentiles from ~~CFSR-the CFSR hindcast~~ and
18 the differences between ~~the CFSR and ERA1 are hindcasts are given~~ in the bottom panels. The medians are clearly different
19 and the ERA1 ~~hindcast~~ is less than ~~CFSR-the CFSR hindcast~~ by 0.1 to 0.4 m ~~aeross-throughout~~ the Arctic. The ~~extreme wave~~

heights-wave heights from the 99th percentile have large differences of 2 m in the area East of Greenland that has significant wave heights larger than 7.5 m. Otherwise the waves in ERAI-the ERAI hindcast are 0.5 m less than CFSR-the CFSR hindcast across the semi-enclosed seas. The top right panel shows the datasets are highly correlated with coefficients larger than 0.95 and exceed 0.98. The Mann-Whitney test reveals that the medians come from different statistical distributions at the 99.9% confidence limit for the entire domain. Therefore we can conclude that the largest differences are in the extreme events but the medians are different as well.

Finally Figure A4 shows the probability distributions using the buoy and altimeter observations are presented in Figure A4. CFSR-of the hindcasts, buoys and altimeters. The CFSR hindcast matches the wave heights larger than 2.5 m well, while ERAI-the ERAI hindcast consistently underestimates. When the H_s is less than 2.5 m CFSR-overestimates more often. ERAI-the CFSR hindcast overestimates. The ERAI hindcast lends to favor the small wave heights. The comparison-to the buoys-buoy comparison in the right panel shows similar features and it is clear that CFSR-. Here the CFSR hindcast overestimates average wave heights of 1-2.5 m which agrees with the examples shown in Figure A1. Therefore we can conclude that the extreme waves and the average conditions are different in the two hindcasts.

In conclusion, both datasets perform reasonably well and their results agree with errors found in the global ocean (Stopa and Cheung, 2014). CFSR-The CFSR wave hindcast consistently predicts higher wave heights for average sea states and matches the upper percentiles much better. Both ERAI and CFSR have better agreement with the measurements between the 10th and 99th percentiles. The upper wave heights in ERAI-the ERAI hindcast diverge from the observations and the 99th percentile has an average bias of 1.5 m. In summary, ERAI-the ERAI hindcast is better suited to describe the average conditions and the 6 hour increment and spatial resolution of 0.7 limits its ability to resolve the peak intensity of the storms. Due to the importance of resolve the upper wave heights we choose CFSR-the CFSR winds to hindcast the entire period from 1992-2014.

Appendix B: Theoretical formulation of friction under ice plates

B1 Extension of the theory by Liu et al.

The representation of dissipative source terms in spectral wave models can generally be cast in a quasi-linear form (Komen et al., 1994)

$$S(f, \theta) = \beta \sigma E(f, \theta), \quad (\text{B1})$$

where $E(f, \theta)$ is the frequency-direction spectrum of the surface elevation, $\sigma = 2\pi f$, and β is a non-dimensional dissipation coefficient that is negative when wave energy is actually dissipated. Previous treatments of the dissipation of wave energy due to friction below an ice layer have been confined to a laminar viscous boundary layer and presented by Liu and Mollo-Christensen (1988),

$$\beta_v = -k \sqrt{\nu \sigma / 2} / (1 + kM), \quad (\text{B2})$$

in which k and σ are the wavenumber and radian frequency, related by a dispersion relation that can be affected by the ice, and M is the ice inertia effect related to the ice thickness multiplied by the ratio of ice to water density. In the present paper, because we focus on the dominant long-period waves, for which the effect of the ice is less, we have used the ice-free dispersion relation $\sigma^2 = gk \tanh(kD)$ in which D is the water depth and g the acceleration of gravity. For these long waves, the factor kM in eq. (B2) can be neglected.

For practical applications, the obtained dissipation coefficient β was then scaled up to fit observed wave attenuations by replacing the molecular viscosity at the freezing temperature of sea water, $\nu \simeq 1.83 \times 10^{-6} \text{ m}^2/\text{s}$ by an eddy viscosity that was proposed to be as large as $0.3 \text{ m}^2/\text{s}$ (Liu et al., 1991). Such a change in viscosity only makes sense if the flow is turbulent. Further, the functional form of the dissipation can be very different for laminar and turbulent frictions in an oscillatory flow near a boundary, as observed by Jensen et al. (1989). In turbulent boundary layers, the energy dissipation coefficient typically grow with the wave amplitude, leading to a dependence of β on the wave amplitude.

We thus revisit this question and propose a parametrization for the laminar to turbulent transition of the boundary layer below the ice. In turbulent conditions, an important parameter is the roughness length below the ice z_0 . That roughness is unfortunately not well known, with only a few measurements of current boundary layers (e.g. McPhee and Smith, 1976). Because the roughness for the wave motion is probably different from the roughness for the currents, as it is well known for ocean bottom boundary layers (Grant and Madsen, 1979), we are left with the difficulty of defining the value of z_0 . Given this roughness, the orbital velocity profile is expected to follow a Kelvin function (Grant and Madsen, 1979) with a dissipation source term that takes a form similar to that of bottom friction (e.g. Madsen et al., 1990; Ardhuin et al., 2003) or swell dissipation by friction at the air-sea interface,

$$\beta_t = -f_e u_{\text{orb}}/g \quad (\text{B3})$$

where the significant orbital amplitudes of the surface velocity is, for deep water waves,

$$u_{\text{orb}} = 2 \sqrt{\int_0^\infty (2\pi f)^2 E(f) df}. \quad (\text{B4})$$

and f_e is the same dissipation factor used for bottom friction, that is a function only of the ratio a_{orb}/z_0 where a_{orb} is the significant orbital displacement at the sea surface, here for deep water waves $a_{\text{orb}} = H_s/2$.

From bottom and air-sea boundary layer studies, the transition from laminar to turbulent is expected to occur for at a threshold Re_c of the significant Reynolds number defined by

$$\text{Re} = u_{\text{orb}} u_{\text{orb}}/\nu. \quad (\text{B5})$$

We take the same critical value $\text{Re}_c = 1.5 \times 10^5$ found for the bottom boundary layer by Jensen et al. (1989) and the air-sea boundary layer by Perignon et al. (2014). Because of the random nature of the waves, with Rayleigh-distributed wave heights, we expect a smooth transition of the average dissipation rate from viscous to turbulent. We found that the average dissipation

caused by random wave heights that follow a Rayleigh distribution is well approximated by the following combined dissipation parameter

$$\beta_c = (1 - w)c_v\beta_v + wc_t\beta_t \quad (\text{B6})$$

in which c_v and c_t are empirical adjustment constants, expected to be close to 1, and the weight w transitions smoothly with the value of Re over a range $\Delta_{\text{Re}} = 200000$,

$$w = 0.5 [1 + \tanh((\text{Re} - \text{Re}_c)/\Delta_{\text{Re}})]. \quad (\text{B7})$$

Figure B shows the expected decay distance as a function of frequency, due to molecular viscosity (blue) or a turbulent boundary layer with a roughness $z_0=0.1$ mm, for significant wave heights ranging from 0.5 to 5 m. In our applications we have chosen $z_0 = 1$ cm.

B2 Empirical adjustment of the wave attenuation

Wadhams and Doble (2009) have reported measurements of waves with periods larger than 20 s far into the ice pack (the periods reported in the paper were erroneously reduced by a factor 1.5, personal communication of M. Doble, 2015). An event with 20 s waves recorded 1400 km into the ice pack on February 13, 2007, had a maximum significant wave height of 3 cm. For this small wave height the wave boundary layer is expected to be laminar. However, using the dissipation coefficient in eq. (B6) produced maximum wave heights of 30 cm. Changing only the coefficient c_v , it was necessary to increase it from 1 to 8 to obtain a reasonable agreement with the data. We have thus used that value to obtain reasonably small wave heights across the Arctic.

However, we note that $c_v = 8$ tends to overestimate the dissipation in the Southern ocean case discussed by Ardhuin et al. (2015), for which $c_v \simeq 2$ is a better adjustment. Such differences could be partly caused by a more complex geometry of older ice in the Arctic, but a four-fold increase of the area of the ice-water interface that could explain this difference is unlikely. It thus appears that the attenuation in the Arctic may be dominated by other processes than under-ice friction, especially when the ice is not broken. Different processes probably produce different distributions of wave heights in the ice. Given the weak energy level back-scattered in the open waters, the details of the wave attenuation process are not likely to affect much our analysis of wave climatology outside of the ice.

4 Appendix C: Percentage of ice-free time

In ~~the manuscript this study~~ we present ice-free ~~statistics. Sea ice is assumed~~ (when the concentration ~~is larger than~~ $\gtrsim 15\%$). ~~The presentation of the~~ statistics. The statistics will vary based on ~~the method used to consider the inclusion of ice conditions how the ice conditions are included~~ in the analysis. ~~Each method of computing wave climate statistics and a number of methods are~~ described by Tuomi et al. (2011) ~~has its own advantages depending on the application. However the~~. The different statistics can be related through the percentage of ice-free time presented in Figure C1. The colorbar is displayed in a logarithmic scale

10 to highlight the details of the small ice percentages while including the regions rarely covered by ice. The Nordic-Greenland
11 Sea is ice-free and the area closest to the North Pole is ice-covered throughout the year. It is clear from this depiction that the
12 largest changes occur in the Beaufort-Chukchi Sea and are ice-free less than 15% of the year above the latitude of 74°.

13 **Appendix D: Relationship with the North Atlantic Oscillation and Pacific Decadal Oscillation**

14 ~~The manuscript~~ This study presents area-average ~~correlations with~~ correlation coefficients computed between monthly H_s and
15 the NAO and PDO ~~to indicate indices to quantify~~ the strength of the relationship. These values can be less for individual time
16 series of each point. Therefore we compute the correlation coefficients between the monthly average ~~Hs~~ H_s and the climate
17 indices for all grid points in Figure D1. This is a more accurate portrait of the strength of the relationship and gives the full
18 ~~spatially~~ spatial distribution. It is clear the NAO has the strongest signature in the Nordic-Greenland Sea and extends into
19 the Barents Sea. The maximum correlation coefficient is 0.48 which is larger than Table 1 which is 0.37. Other regions have
20 reduced ~~values of correlations~~ correlation coefficients and are not spatially homogeneous. The PDO has been largely negative
21 for the past decade and is creating the negative correlation coefficients across the Arctic. It is interesting to see that the largest
22 relationship occurs in the Barents Sea ($R=-0.46$) which the area-average results are much less ($R=0.1$). Only a weak relationship
23 exists in the Beaufort-Chukchi Sea contrary to what Frey et al. (2015) showed for the ice and wind field.

24 *Acknowledgements.* This work was supported by LabexMER through grant ANR-10-LABX-19. The CFSR and ERAI reanalysis data is
25 publicly available from rda.ucar.edu and the IFREMER/CERSAT sea ice concentration is available from ftp.ifremer.fr/ifremer/cersat/.

26 References

- 27 Anderson, J. D., Wu, C. H., and Schwab, D. J.: Wave climatology in the Apostle Islands, Lake Superior, *Journal of Geophysical Research:*
28 *Oceans*, 120, 4869–4890, doi:10.1002/2014jc010278, <http://dx.doi.org/10.1002/2014JC010278>, 2015.
- 29 Ardhuin, F., Herbers, T. H. C., Jessen, P. F., and O'Reilly, W. C.: Swell transformation across the continental shelf. part II: validation of a
30 spectral energy balance equation, *J. Phys. Oceanogr.*, 33, 1940–1953, 2003.
- 31 Ardhuin, F., Rogers, E., Babanin, A. V., Filipot, J.-F., Magne, R., Roland, A., van der Westhuysen, A., Queffelecoulou, P., Lefevre, J.-M., Aouf,
32 L., and et al.: Semiempirical Dissipation Source Functions for Ocean Waves. Part I: Definition, Calibration, and Validation, *Journal of*
33 *Physical Oceanography*, 40, 1917–1941, doi:10.1175/2010jpo4324.1, <http://dx.doi.org/10.1175/2010JPO4324.1>, 2010.
- 34 Ardhuin, F., Collard, F., Chapron, B., Girard-Ardhuin, F., Guitton, G., Mouche, A., and Stopa, J. E.: Estimates of ocean wave heights and
35 attenuation in sea ice using the sar wave mode on sentinel1-A, *Geophys. Res. Lett.*, 42, doi:10.1002/2014GL062940, 2015.
- 36 Cavalieri, D. J. and Parkinson, C. L.: Arctic sea ice variability and trends, 1979–2010, *The Cryosphere*, 6, 881–889, doi:10.5194/tc-
37 6-881-2012, <http://dx.doi.org/10.5194/tc-6-881-2012>, 2012.
- 1 Chawla, A., Spindler, D. M., and Tolman, H. L.: Validation of a thirty year wave hindcast using the Climate Forecast System Reanalysis
2 winds, *Ocean Modelling*, 70, 189–206, doi:10.1016/j.ocemod.2012.07.005, <http://dx.doi.org/10.1016/j.ocemod.2012.07.005>, 2013.
- 3 Chen, G., Chapron, B., Ezraty, R., and Vandemark, D.: A Global View of Swell and Wind Sea Climate in the Ocean
4 by Satellite Altimeter and Scatterometer, *Journal of Atmospheric and Oceanic Technology*, 19, 1849–1859, doi:10.1175/1520-
5 0426(2002)019<1849:agvosa>2.0.co;2, [http://dx.doi.org/10.1175/1520-0426\(2002\)019<1849:AGVOSA>2.0.CO;2](http://dx.doi.org/10.1175/1520-0426(2002)019<1849:AGVOSA>2.0.CO;2), 2002.
- 6 Comiso, J. C., Parkinson, C. L., Gersten, R., and Stock, L.: Accelerated decline in the Arctic sea ice cover, *Geophysical Research Letters*,
7 35, doi:10.1029/2007gl031972, <http://dx.doi.org/10.1029/2007GL031972>, 2008.
- 8 Davis, P. E. D., Lique, C., Johnson, H. L., and Guthrie, J. D.: Competing Effects of Elevated Vertical Mixing and Increased Freshwater Input
9 on the Stratification and Sea Ice Cover in a Changing Arctic Ocean, *Journal of Physical Oceanography*, 46, 1531–1553, doi:10.1175/jpo-
10 d-15-0174.1, <http://dx.doi.org/10.1175/JPO-D-15-0174.1>, 2016.
- 11 Dee, D. P., Uppala, S. M., Simmons, A. J., Berrisford, P., Poli, P., Kobayashi, S., Andrae, U., Balmaseda, M. A., Balsamo, G., Bauer, P., and
12 et al.: The ERA-Interim reanalysis: configuration and performance of the data assimilation system, *Q.J.R. Meteorol. Soc.*, 137, 553–597,
13 doi:10.1002/qj.828, <http://dx.doi.org/10.1002/qj.828>, 2011.
- 14 Dobrynin, M., Murawsky, J., and Yang, S.: Evolution of the global wind wave climate in CMIP5 experiments, *Geophysical Research Letters*,
15 39, n/a–n/a, doi:10.1029/2012gl052843, <http://dx.doi.org/10.1029/2012gl052843>, 2012.
- 16 Ezraty, R., Girard-Ardhuin, F., Piolle, J. F., Kaleschke, L., and Heygster, G.: Arctic and Antarctic sea ice concentration
17 and Arctic sea ice drift estimated from Special Sensors Microwave data, User manual version 2.1, Ifremer/CERSAT,
18 <ftp.ifremer.fr/ifremer/cersat/products/gridded/psi-drift/documentation/ssmi.pdf>, [ftp://ftp.ifremer.fr/ifremer/cersat/products/gridded/](ftp://ftp.ifremer.fr/ifremer/cersat/products/gridded/psi-drift/documentation/ssmi.pdf)
19 [psi-drift/documentation/ssmi.pdf](ftp://ftp.ifremer.fr/ifremer/cersat/products/gridded/psi-drift/documentation/ssmi.pdf), 2007.
- 20 Francis, O. P., Panteleev, G. G., and Atkinson, D. E.: Ocean wave conditions in the Chukchi Sea from satellite and in situ observations,
21 *Geophysical Research Letters*, 38, n/a–n/a, doi:10.1029/2011gl049839, <http://dx.doi.org/10.1029/2011GL049839>, 2011.
- 22 Frey, K., Moore, G. W. K., Cooper, L. W., and Grebmeier, J. M.: Divergent patterns of recent sea ice cover cross the Bering, Chukchi, and
23 Beaufort seas of the Pacific Arctic Region, *Progress in Oceanography*, 136, 32–49, doi:10.1016/j.pocean.2015.05.009, 2015.
- 24 Gemmrich, J., Thomas, B., and Bouchard, R.: Observational changes and trends in northeast Pacific wave records, *Geophysical Research*
25 *Letters*, 38, n/a–n/a, doi:10.1029/2011gl049518, <http://dx.doi.org/10.1029/2011GL049518>, 2011.

26 Grant, W. D. and Madsen, O. S.: Combined wave and current interaction with a rough bottom, *J. Geophys. Res.*, 84, 1797–1808, 1979.

27 Gulev, S. K. and Grigorieva, V.: Variability of the Winter Wind Waves and Swell in the North Atlantic and North Pacific as Revealed by the
28 Voluntary Observing Ship Data, *J. Climate*, 19, 5667–5685, doi:10.1175/jcli3936.1, <http://dx.doi.org/10.1175/JCLI3936.1>, 2006.

29 Hanson, J. L. and Phillips, O. M.: Automated Analysis of Ocean Surface Directional Wave Spectra, *Journal of Atmospheric and*
30 *Oceanic Technology*, 18, 277–293, doi:10.1175/1520-0426(2001)018<0277:aaosd>2.0.co;2, [http://dx.doi.org/10.1175/1520-0426\(2001\)](http://dx.doi.org/10.1175/1520-0426(2001)018<0277:AAOOSD>2.0.CO;2)
31 [018<0277:AAOOSD>2.0.CO;2](http://dx.doi.org/10.1175/1520-0426(2001)018<0277:AAOOSD>2.0.CO;2), 2001.

32 Hartmann, D., Tank, A. K., Rusticucci, M., Alexander, L., Bronnimann, S., Charabi, Y., Dentener, F., Dlugokencky, E., Easterling, D., Kaplan,
33 A., Soden, B., Thorne, P., Wild, M., and Zhai, P.: Observations: Atmosphere and Surface. In: *Climate Change 2013: The Physical Science*
34 *Basis*, Cambridge University Press, Cambridge, United Kingdom and New York, NY, USA., 2013.

35 Hirsch, R. M., Slack, J. R., and Smith, R. A.: Techniques of trend analysis for monthly water quality data, *Water Resour. Res.*, 18, 107–121,
36 doi:10.1029/wr018i001p00107, <http://dx.doi.org/10.1029/WR018i001p00107>, 1982.

37 Husson, R., Ardhuin, F., Collard, F., Chapron, B., and Balanche, A.: Revealing forerunners on Envisat’s wave mode ASAR using the Global
1 Seismic Network, *Geophysical Research Letters*, 39, n/a–n/a, doi:10.1029/2012gl052334, <http://dx.doi.org/10.1029/2012GL052334>,
2 2012.

3 Jeffries, M. O., Overland, J. E., and Perovich, D. K.: The Arctic shifts to a new normal, *Physics Today*, 66, 35, doi:10.1063/pt.3.2147,
4 <http://dx.doi.org/10.1063/PT.3.2147>, 2013.

5 Jensen, B. L., Sumer, B. M., and Fredsoe, J.: Turbulent oscillatory boundary layers at high Reynolds numbers, *J. Fluid Mech.*, 206, 265–297,
6 1989.

7 Kaleschke, L., Lupkes, C., Vihma, T., Haarpaintner, J., Bochert, A., Hartmann, J., and Heygster, G.: SSM/I Sea Ice Re-
8 mote Sensing for Mesoscale Ocean-Atmosphere Interaction Analysis, *Canadian Journal of Remote Sensing*, 27, 526–537,
9 doi:10.1080/07038992.2001.10854892, <http://dx.doi.org/10.1080/07038992.2001.10854892>, 2001.

10 Kendall, M.: *Rank Correlation Methods*, 4th edition, Oxford University Press, 1975.

11 Khon, V. C., Mokhov, I. I., Pogarskiy, F. A., Babanin, A., Dethloff, K., Rinke, A., and Matthes, H.: Wave heights in the 21 st century
12 Arctic Ocean simulated with a regional climate model, *Geophysical Research Letters*, 41, 2956–2961, doi:10.1002/2014gl059847, <http://dx.doi.org/10.1002/2014GL059847>,
13 <http://dx.doi.org/10.1002/2014GL059847>, 2014.

14 Kohout, A. L., Williams, M. J. M., Dean, S. M., and Meylan, M. H.: Storm-induced sea-ice breakup and the implications for ice extent,
15 *Nature*, 509, 604–607, doi:10.1038/nature13262, <http://dx.doi.org/10.1038/nature13262>, 2014.

16 Komen, G. J., Cavaleri, L., Donelan, M., Hasselmann, K., Hasselmann, S., and Janssen, P. A. E. M.: *Dynamics and modelling of ocean*
17 *waves*, Cambridge University Press, 1994.

18 Li, J., Kohout, A. L., and Shen, H. H.: Comparison of wave propagation through ice covers in calm and storm conditions, *Geophysical*
19 *Research Letters*, 42, 5935–5941, doi:10.1002/2015gl064715, <http://dx.doi.org/10.1002/2015GL064715>, 2015.

20 Liu, A. K. and Cavalieri, D. J.: On sea ice drift from the wavelet analysis of the Defense Meteorological Satellite Program (DMSP) Special
21 Sensor Microwave Imager (SSM/I) data, *International Journal of Remote Sensing*, 19, 1415–1423, doi:10.1080/014311698215522, <http://dx.doi.org/10.1080/014311698215522>,
22 <http://dx.doi.org/10.1080/014311698215522>, 1998.

23 Liu, A. K. and Mollo-Christensen, E.: Wave propagation in a solid ice pack, *J. Phys. Oceanogr.*, 18, 1702–1712, 1988.

24 Liu, A. K., Holt, B., and Vachon, P. W.: Wave propagation in the marginal ice zone’ model predictions and comparisons with buoy and
25 synthetic aperture radar data, *J. Geophys. Res.*, 96, 4605–4621, 1991.

- 26 Madsen, O. S., Mathisen, P. P., and Rosengaus, M. M.: Movable bed friction factors for spectral waves, in: Proceedings of the 22nd interna-
27 tional conference on coastal engineering, ASCE, pp. 420–429, 1990.
- 28 Mann, H. B.: Nonparametric tests against trend, *Econometrica*, 13, 245–259, <http://www.jstor.org/stable/1907187>, 1945.
- 29 Marko, J. R.: Observations and analyses of an intense waves-in-ice event in the Sea of Okhotsk, *Journal of Geophysical Research*, 108,
30 doi:10.1029/2001jc001214, <http://dx.doi.org/10.1029/2001JC001214>, 2003.
- 31 McPhee, M. G. and Smith, J. D.: Measurements of the turbulent boundary layer under pack ice, *J. Phys. Oceanogr.*, 6, 696–711, 1976.
- 32 Overeem, I., Anderson, R. S., Wobus, C. W., Clow, G. D., Urban, F. E., and Matell, N.: Sea ice loss enhances wave action at the Arctic coast,
33 *Geophysical Research Letters*, 38, n/a–n/a, doi:10.1029/2011gl048681, <http://dx.doi.org/10.1029/2011GL048681>, 2011.
- 34 Perignon, Y., Ardhuin, F., Cathelain, M., and Robert, M.: Swell dissipation by induced atmospheric shear stress, *J. Geophys. Res.*, 119,
35 6622–6630, doi:10.1002/2014JC009896, 2014.
- 36 Perovich, D.: The Changing Arctic Sea Ice Cover, *Oceanography*, 24, 162–173, doi:10.5670/oceanog.2011.68, <http://dx.doi.org/10.5670/>
37 [oceanog.2011.68](http://dx.doi.org/10.5670/oceanog.2011.68), 2011.
- 38 Pierson, W. J. and Moskowitz, L.: A proposed spectral form for fully developed wind seas based on the similarity theory of S. A. Kitaig-
1 orodskii, *Journal of Geophysical Research*, 69, 5181–5190, doi:10.1029/jz069i024p05181, <http://dx.doi.org/10.1029/JZ069i024p05181>,
2 1964.
- 3 Popova, E. E., Yool, A., Coward, A. C., Aksenov, Y. K., Alderson, S. G., de Cuevas, B. A., and Anderson, T. R.: Control of primary
4 production in the Arctic by nutrients and light: insights from a high resolution ocean general circulation model, *Biogeosciences*, 7,
5 3569–3591, doi:10.5194/bg-7-3569-2010, <http://dx.doi.org/10.5194/bg-7-3569-2010>, 2010.
- 6 Queffelecoul, P. and Croize-Fillon, D.: Global altimeter SWH data set, Technical Report 11.1, IFREMER/CERSAT, [ftp://ftp.ifremer.fr/ifremer/](ftp://ftp.ifremer.fr/ifremer/cersat/products/swath/altimeters/waves/documentation/altimeter_wave_merge__11.1.pdf)
7 [cersat/products/swath/altimeters/waves/documentation/altimeter_wave_merge__11.1.pdf](ftp://ftp.ifremer.fr/ifremer/cersat/products/swath/altimeters/waves/documentation/altimeter_wave_merge__11.1.pdf), 2015.
- 8 Rasclé, N. and Ardhuin, F.: A global wave parameter database for geophysical applications. Part 2: Model validation with improved source
9 term parameterization, *Ocean Modelling*, 70, 174–188, doi:10.1016/j.ocemod.2012.12.001, <http://dx.doi.org/10.1016/j.ocemod.2012.12>.
10 001, 2013.
- 11 Reistad, M., Breivik, O., Haakenstad, H., Aarnes, O. J., Furevik, B. R., and Bidlot, J.-R.: A high-resolution hindcast of wind and waves
12 for the North Sea, the Norwegian Sea, and the Barents Sea, *Journal of Geophysical Research*, 116, doi:10.1029/2010jc006402, <http://dx.doi.org/10.1029/2010JC006402>, 2011.
- 14 Rogers, E. W. and Orzech, M. D.: Implementation and testing of ice and mud source functions in WAVEWATCH III, Memorandum Report
15 NLR/MR/7320-13-9462, Naval Research Laboratory, <http://www7320.nrlssc.navy.mil/pubs.php>, 2013.
- 16 Saha, S., Moorthi, S., Pan, H.-L., Wu, X., Wang, J., Nadiga, S., Tripp, P., Kistler, R., Woollen, J., Behringer, D., and et al.: The NCEP
17 Climate Forecast System Reanalysis, *Bulletin of the American Meteorological Society*, 91, 1015–1057, doi:10.1175/2010bams3001.1,
18 <http://dx.doi.org/10.1175/2010BAMS3001.1>, 2010.
- 19 Saha, S., Moorthi, S., Wu, X., Wang, J., Nadiga, S., Tripp, P., Behringer, D., Hou, Y.-T., Chuang, H.-y., Iredell, M., and et al.: The NCEP Cli-
20 mate Forecast System Version 2, *J. Climate*, 27, 2185–2208, doi:10.1175/jcli-d-12-00823.1, <http://dx.doi.org/10.1175/JCLI-D-12-00823>.
21 1, 2014.
- 22 Screen, J. A. and Simmonds, I.: The central role of diminishing sea ice in recent Arctic temperature amplification, *Nature*, 464, 1334–1337,
23 doi:10.1038/nature09051, <http://dx.doi.org/10.1038/nature09051>, 2010.
- 24 Semedo, A., Sušelj, K., Rutgersson, A., and Sterl, A.: A Global View on the Wind Sea and Swell Climate and Variability from ERA-40, *J.*
25 *Climate*, 24, 1461–1479, doi:10.1175/2010jcli3718.1, <http://dx.doi.org/10.1175/2010JCLI3718.1>, 2011.

26 Semedo, A., Vettor, R., Breivik, O., Sterl, A., Reistad, M., Soares, C. G., and Lima, D.: The wind sea and swell waves climate in the Nordic
27 seas, *Ocean Dynamics*, 65, 223–240, doi:10.1007/s10236-014-0788-4, <http://dx.doi.org/10.1007/s10236-014-0788-4>, 2014.

28 Sen, P. K.: Estimates of the Regression Coefficient Based on Kendall's Tau, *Journal of the American Statistical Association*, 63, 1379–1389,
29 doi:10.1080/01621459.1968.10480934, <http://dx.doi.org/10.1080/01621459.1968.10480934>, 1968.

30 Sepulveda, H. H., Queffelec, P., and Ardhuin, F.: Assessment of SARAL/AltiKa Wave Height Measurements Relative to Buoy, Jason-
31 2, and Cryosat-2 Data, *Marine Geodesy*, 38, 449–465, doi:10.1080/01490419.2014.1000470, [http://dx.doi.org/10.1080/01490419.2014.](http://dx.doi.org/10.1080/01490419.2014.1000470)
32 1000470, 2015.

33 Simmonds, I. and Rudeva, I.: The great Arctic cyclone of August 2012, *Geophysical Research Letters*, 39, doi:10.1029/2012gl054259,
34 <http://dx.doi.org/10.1029/2012GL054259>, 2012.

35 Smith, M. and Thomson, J.: Scaling observations of surface waves in the Beaufort Sea, *Elementa: Science of the Anthropocene*, 4, 000 097,
36 doi:10.12952/journal.elementa.000097, <http://dx.doi.org/10.12952/journal.elementa.000097>, 2016.

37 Squire, V.: Of ocean waves and sea-ice revisited, *Cold Regions Science and Technology*, 49, 110–133,
1 doi:10.1016/j.coldregions.2007.04.007, <http://dx.doi.org/10.1016/j.coldregions.2007.04.007>, 2007.

2 Squire, V. A., Dugan, J. P., Wadhams, P., Rottier, P. J., and Liu, A. K.: Of Ocean Waves and Sea Ice, *Annual Review of Fluid Mechanics*, 27,
3 115–168, doi:10.1146/annurev.fl.27.010195.000555, <http://dx.doi.org/10.1146/annurev.fl.27.010195.000555>, 1995.

4 Steele, M., Ermold, W., and Zhang, J.: Arctic Ocean surface warming trends over the past 100 years, *Geophysical Research Letters*, 35,
5 doi:10.1029/2007gl031651, <http://dx.doi.org/10.1029/2007GL031651>, 2008.

6 Stephenson, S. R., Smith, L. C., and Agnew, J. A.: Divergent long-term trajectories of human access to the Arctic, *Nature Climate change*,
7 1, 156–160, doi:10.1038/nclimate1120, <http://dx.doi.org/10.1038/nclimate1120>, 2011.

8 Sterl, A. and Caires, S.: Climatology, variability and extrema of ocean waves: the Web-based KNMI/ERA-40 wave atlas, *Int. J. Climatol.*,
9 25, 963–977, doi:10.1002/joc.1175, <http://dx.doi.org/10.1002/joc.1175>, 2005.

10 Stopa, J. E. and Cheung, K. F.: Intercomparison of wind and wave data from the ECMWF Reanalysis Interim and the NCEP Climate Forecast
11 System Reanalysis, *Ocean Modelling*, 75, 65–83, doi:10.1016/j.ocemod.2013.12.006, <http://dx.doi.org/10.1016/j.ocemod.2013.12.006>,
12 2014.

13 Stopa, J. E., Cheung, K. F., Tolman, H. L., and Chawla, A.: Patterns and cycles in the Climate Forecast System Reanalysis wind and wave
14 data, *Ocean Modelling*, 70, 207–220, doi:10.1016/j.ocemod.2012.10.005, <http://dx.doi.org/10.1016/j.ocemod.2012.10.005>, 2013a.

15 Stopa, J. E., Filipot, J.-F., Li, N., Cheung, K. F., Chen, Y.-L., and Vega, L.: Wave energy resources along the Hawaiian Island chain, *Renewable*
16 *Energy*, 55, 305–321, doi:10.1016/j.renene.2012.12.030, <http://dx.doi.org/10.1016/j.renene.2012.12.030>, 2013b.

17 Stopa, J. E., Ardhuin, F., Babanin, A., and Zieger, S.: Comparison and validation of physical wave parameterizations in spectral wave models,
18 *Ocean Modelling*, doi:10.1016/j.ocemod.2015.09.003, <http://dx.doi.org/10.1016/j.ocemod.2015.09.003>, 2015.

19 Thomson, J. and Rogers, W. E.: Swell and sea in the emerging Arctic Ocean, *Geophysical Research Letters*, 41, 3136–3140,
20 doi:10.1002/2014gl059983, <http://dx.doi.org/10.1002/2014GL059983>, 2014.

21 Thomson, J. and Team, D.: Emerging trends in the sea state of the Beaufort and Chukchi Seas, *Ocean Modelling*, 2016.

22 Tolman, H. L.: Alleviating the Garden Sprinkler Effect in wind wave models, *Ocean Modelling*, 4, 269–289, doi:10.1016/s1463-
23 5003(02)00004-5, [http://dx.doi.org/10.1016/S1463-5003\(02\)00004-5](http://dx.doi.org/10.1016/S1463-5003(02)00004-5), 2002.

24 Tolman, H. L. and the WAVEWATCH III Development Group: User Manual and system documentation of WAVEWATCH III version 4.18,
25 Technical Note 316, NOAA/NWS/NCEP/MMAB, 2014.

26 Tolman, H. L., Banner, M. L., and Kaihatu, J. M.: The NOPP operational wave model improvement project, *Ocean Modelling*, 70, 2–10,
 755 doi:10.1016/j.ocemod.2012.11.011, <http://dx.doi.org/10.1016/j.ocemod.2012.11.011>, 2013.

756 Tremblay, J.-E., Simpson, K., Martin, J., Miller, L., Gratton, Y., Barber, D., and Price, N. M.: Vertical stability and the annual dy-
 757 namics of nutrients and chlorophyll fluorescence in the coastal, southeast Beaufort Sea, *Journal of Geophysical Research*, 113,
 758 doi:10.1029/2007jc004547, <http://dx.doi.org/10.1029/2007JC004547>, 2008.

759 Tuomi, L., Kahma, K. K., and Pettersson, H.: Wave hindcast statistics in the seasonseas ice-covered Baltic Sea, *Boreal Environment Research*,
 760 16, 451–472, 2011.

761 Uppala, S. M., Kallberg, P. W., Simmons, A. J., Andrae, U., Bechtold, V. D. C., Fiorino, M., Gibson, J. K., Haseler, J., Hernandez, A., Kelly,
 762 G. A., and et al.: The ERA-40 re-analysis, *Q.J.R. Meteorol. Soc.*, 131, 2961–3012, doi:10.1256/qj.04.176, <http://dx.doi.org/10.1256/qj.04.176>,
 763 176, 2005.

764 Wadhams, P. and Doble, M. J.: Sea ice thickness measurement using episodic infragravity waves from distant storms, *Cold Regions Science*
 765 and Technology, 56, 98–101, doi:10.1016/j.coldregions.2008.12.002, <http://dx.doi.org/10.1016/j.coldregions.2008.12.002>, 2009.

766 Wang, X. L. and Swail, V. R.: Changes of Extreme Wave Heights in Northern Hemisphere Oceans and Related Atmospheric
 767 Circulation Regimes, *J. Climate*, 14, 2204–2221, doi:10.1175/1520-0442(2001)014<2204:coewhi>2.0.co;2, [http://dx.doi.org/10.1175/1520-0442\(2001\)014<2204:COEWHI>2.0.CO;2](http://dx.doi.org/10.1175/1520-0442(2001)014<2204:COEWHI>2.0.CO;2), 2001.

769 Wang, X. L., Feng, Y., Swail, V. R., and Cox, A.: Historical Changes in the Beaufort–Chukchi–Bering Seas Surface Winds and Waves,
 770 1971–2013, *J. Climate*, 28, 7457–7469, doi:10.1175/jcli-d-15-0190.1, <http://dx.doi.org/10.1175/JCLI-D-15-0190.1>, 2015.

771 Young, I. R., Zieger, S., and Babanin, A. V.: Global Trends in Wind Speed and Wave Height, *Science*, 332, 451–455,
 772 doi:10.1126/science.1197219, <http://dx.doi.org/10.1126/science.1197219>, 2011.

773 Zhang, J.: Warming of the arctic ice-ocean system is faster than the global average since the 1960s, *Geophysical Research Letters*, 32,
 774 doi:10.1029/2005gl024216, <http://dx.doi.org/10.1029/2005GL024216>, 2005.

775 Zhang, J., Lindsay, R., Schweiger, A., and Steele, M.: The impact of an intense summer cyclone on 2012 Arctic sea ice retreat, *Geophys.*
 776 *Res. Lett.*, 40, 720–726, doi:10.1002/grl.50190, <http://dx.doi.org/10.1002/grl.50190>, 2013.

777 Zieger, S., Vinoth, J., and Young, I. R.: Joint Calibration of Multiplatform Altimeter Measurements of Wind Speed and Wave Height over
 778 the Past 20 Years, *Journal of Atmospheric and Oceanic Technology*, 26, 2549–2564, doi:10.1175/2009jtecha1303.1, <http://dx.doi.org/10.1175/2009JTECHA1303.1>, 2009.

Table 1. Correlation coefficients and trends for the various regions and parameters. The correlations coefficients are given between area-averaged monthly time series versus the North Atlantic Oscillation and the Pacific Decadal Oscillation in parentheses. Statistically significant results are given by the '*' when the p-value is less than 0.05.

Region	Avr Ocean Area	U10 _{Avr}	U10 _{P95}	H _{sAvr}	H _{sP95}
Arctic Ocean	-0.19*(-0.25*)	+0.37*(-0.02)	+0.35*(-0.08)	+0.31*(-0.02)	+0.31*(-0.08)
Nordic-Greenland Sea	-0.10 (-0.27*)	+0.37*(-0.09)	+0.35*(-0.11)	+0.32*(-0.08)	+0.33*(-0.13*)
Barents Sea	-0.15*(-0.33*)	+0.29*(-0.10)	+0.29*(-0.12*)	+0.22*(-0.04)	+0.22*(-0.10)
Kara Sea	-0.15*(-0.16*)	+0.19*(-0.20*)	+0.16*(-0.20*)	+0.11 (-0.10)	+0.05 (-0.14*)
Laptev Sea	+0.15 (-0.27*)	-0.01 (-0.11)	-0.01 (-0.09)	-0.12 (+0.06)	-0.08 (+0.01)
E. Siberia Sea	+0.17 (-0.13)	+0.01 (-0.08)	+0.02 (-0.06)	-0.12 (+0.14)	-0.01 (+0.13)
Beaufort-Chukchi Sea	-0.03 (-0.24*)	+0.05 (-0.21*)	-0.00 (-0.21*)	+0.05 (-0.15)	+0.00 (-0.17*)
Baffin Bay	-0.12 (-0.19*)	-0.07 (-0.16*)	-0.09 (-0.15*)	+0.10 (-0.11)	+0.08 (-0.13)

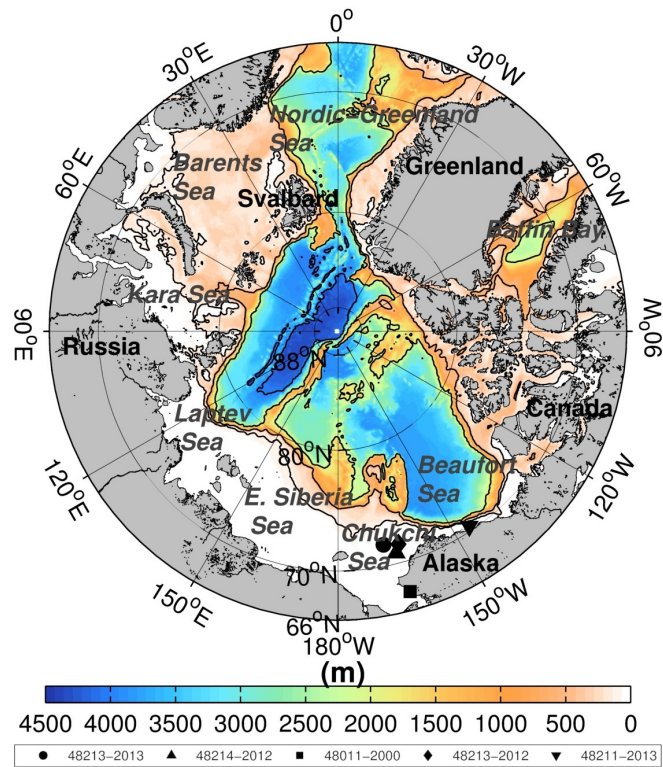


Figure 1. Regional seas of the Arctic Ocean ~~colors respond to depth and with bathymetry (color)~~, buoy locations ~~are plotted in magenta~~ (black symbols), and 4000, 2000, 500, and 100 m depth contours (black lines)

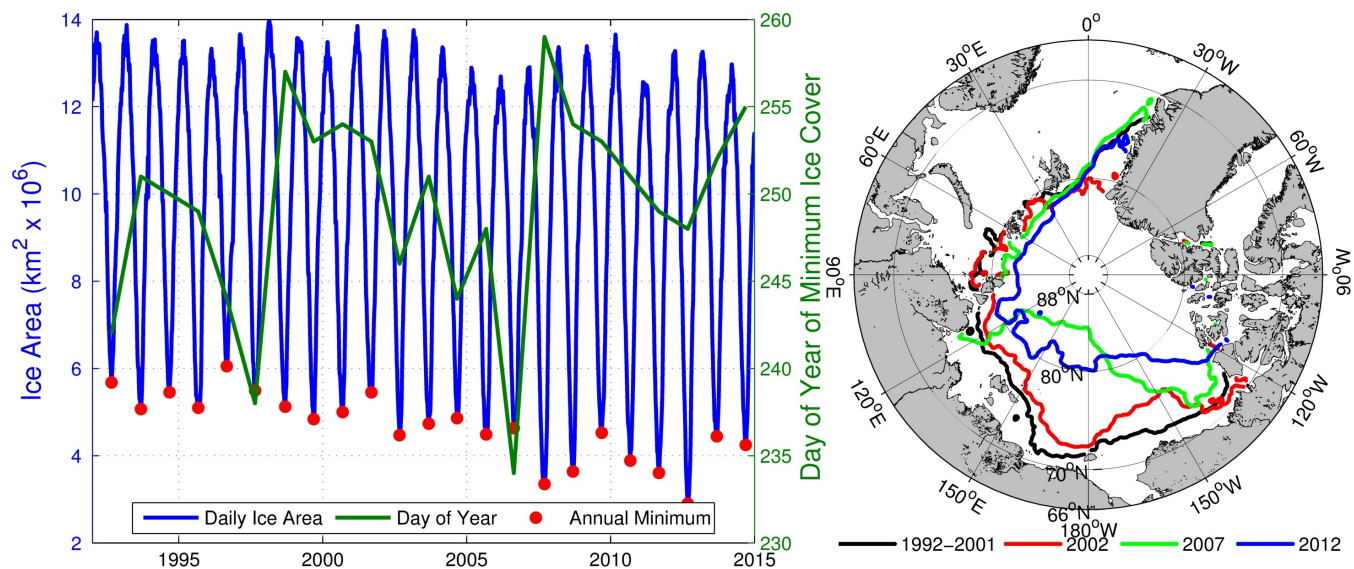


Figure 2. Daily SSM/I Ifremer CERSAT ice area (concentrations 1992-2014). The left panel displays the ice coverage in area minimum assuming for 1992-2001 grid points with a concentration greater than 15% (represents the median), 2002, 2007, and 2012 minimum of the day of the year (right) from the Ifremer/CERSAT ice concentrations. The right panel shows the minimum spatial ice edge is defined as by the 15% ice concentration contour for 1992-2001 (median), 2002, 2007, and 2012.

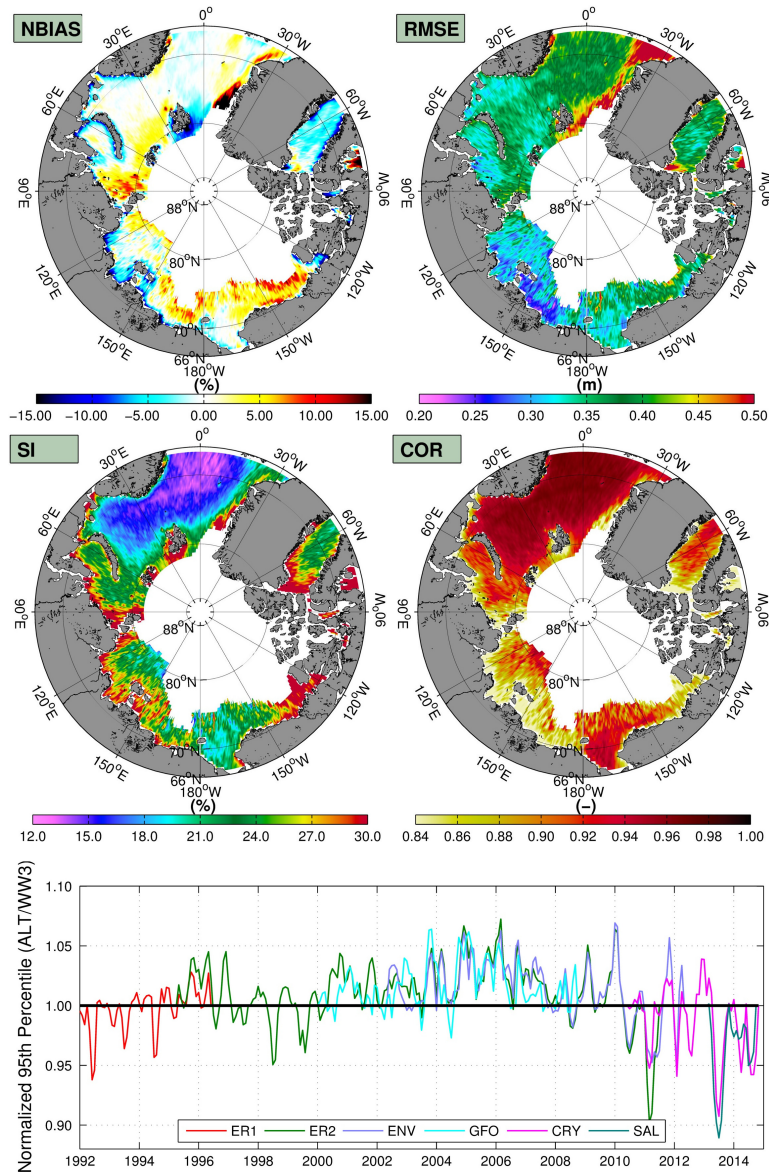


Figure 3. Normalized Top four panels display the normalized bias (NBIAS), root mean squared error (RMSE), scatter index (SI), and correlation coefficient (COR) for collocated significant wave heights H_s for the CFSR wave hindcast and the merged altimeters 1992-2014 (top four panels). The bottom panel displays the normalized monthly H_s 95th percentile for each satellite platform: European Remote Sensing Satellites 1 and 2 (ER1, ER2), Environmental Satellite ENVISAT (ENV), Geosat Follow-On (GFO), CRYOSAT2 (CRY), and AltiKa SARAL (SAL).

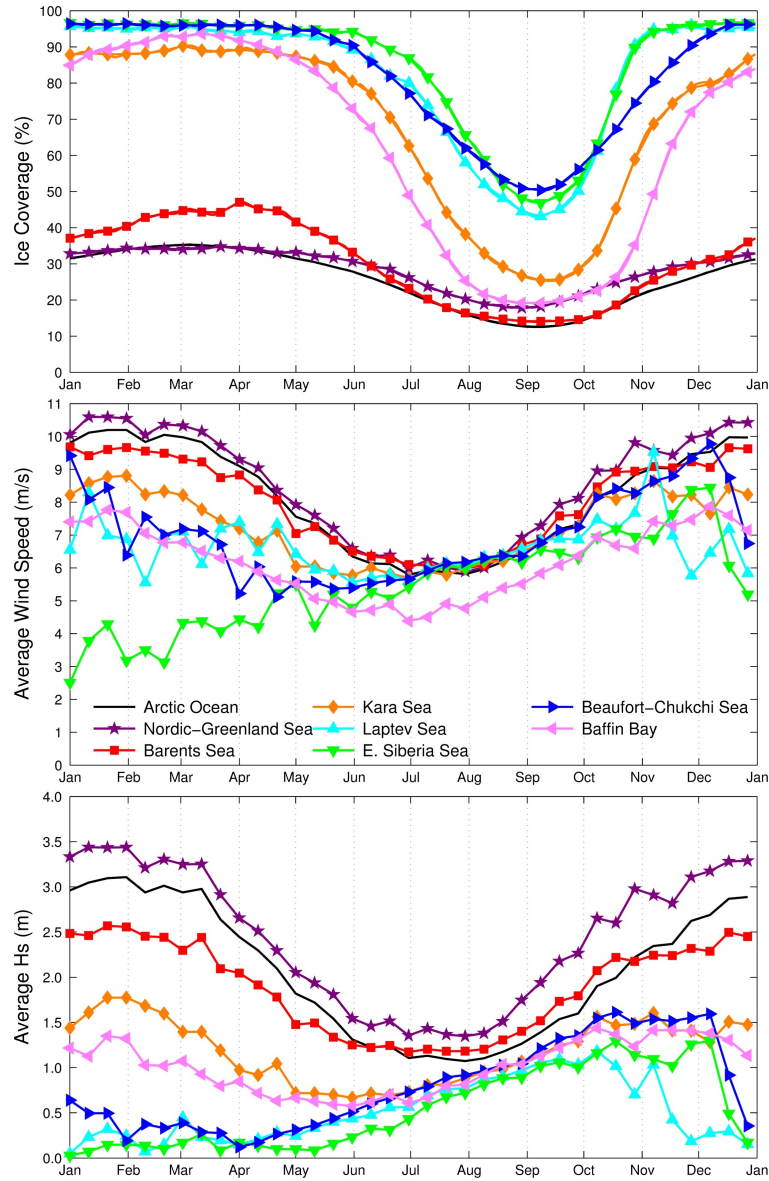


Figure 4. Daily-averaged-ice coverage (top), wind speed (middle), and significant-wave heights- H_s daily averages computed from a spatial average for different regions of the each Arctic illustrating region showing the seasonality.

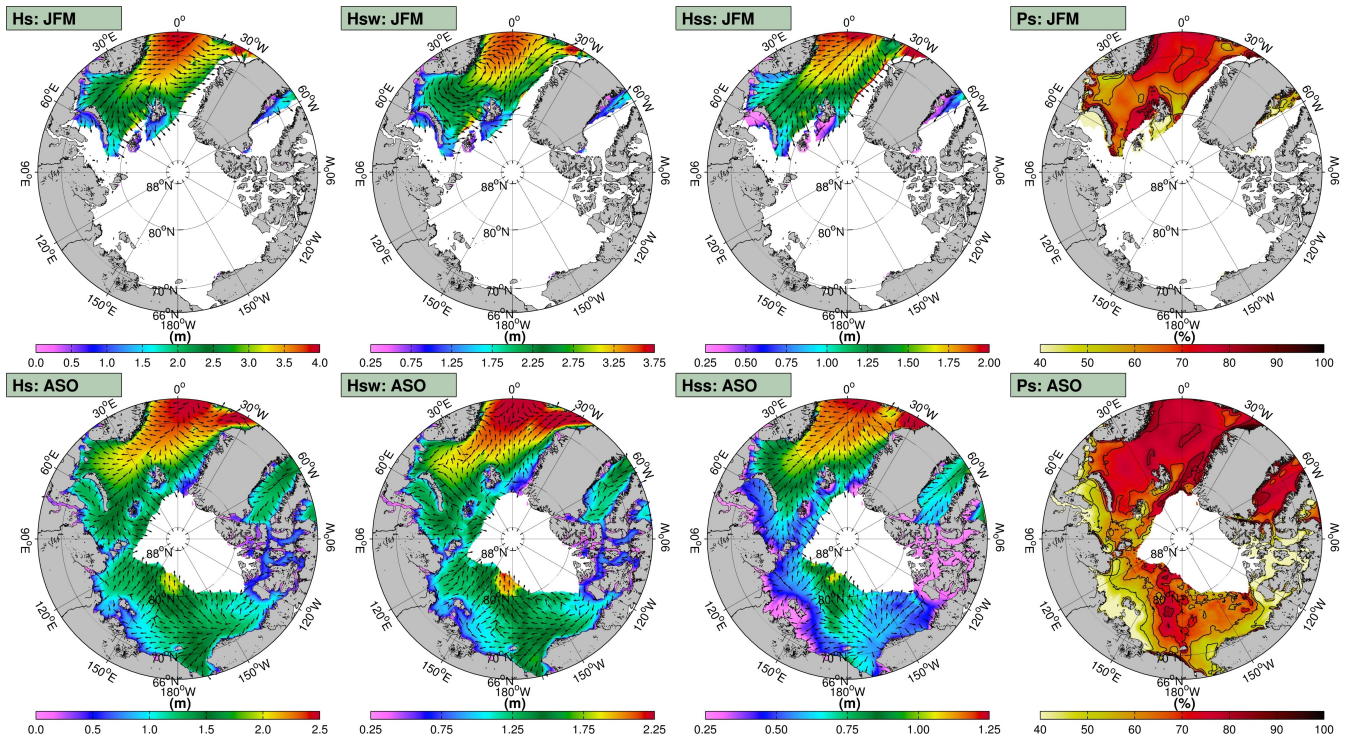


Figure 5. January-February-March (JFM) and August-September-October (ASO) seasonal averages of significant wave height H_s (first column), wind-sea wave height H_{sw} (second column), swell wave height H_{ss} (third column), and swell persistence P_s (fourth column). The directions are computed from by averaging the east-west and north-south components separately.

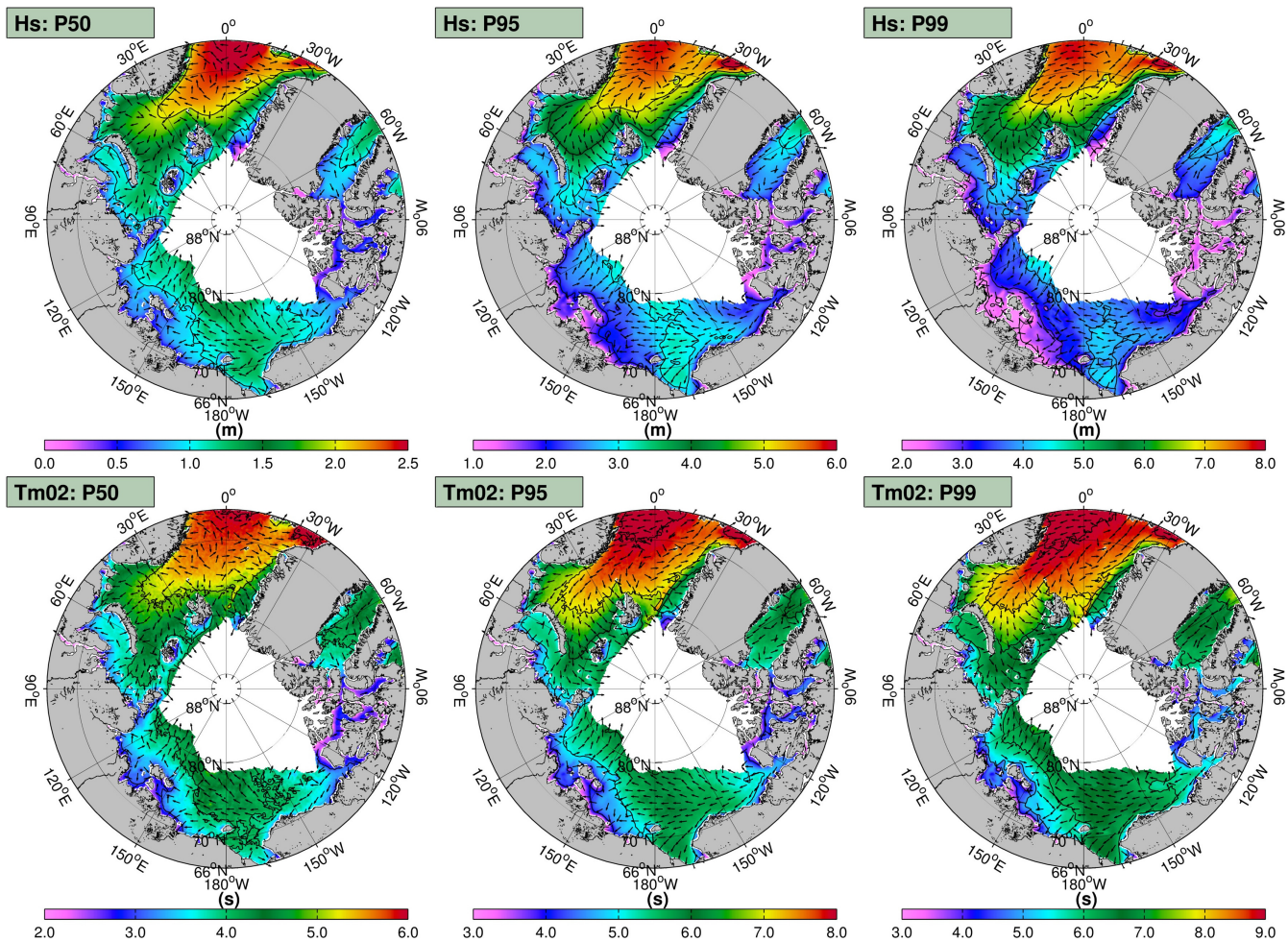


Figure 6. Significant wave height percentiles (top panels) with-matching-and-corresponding-averaged wave periods (bottom panels) and directions (arrows).

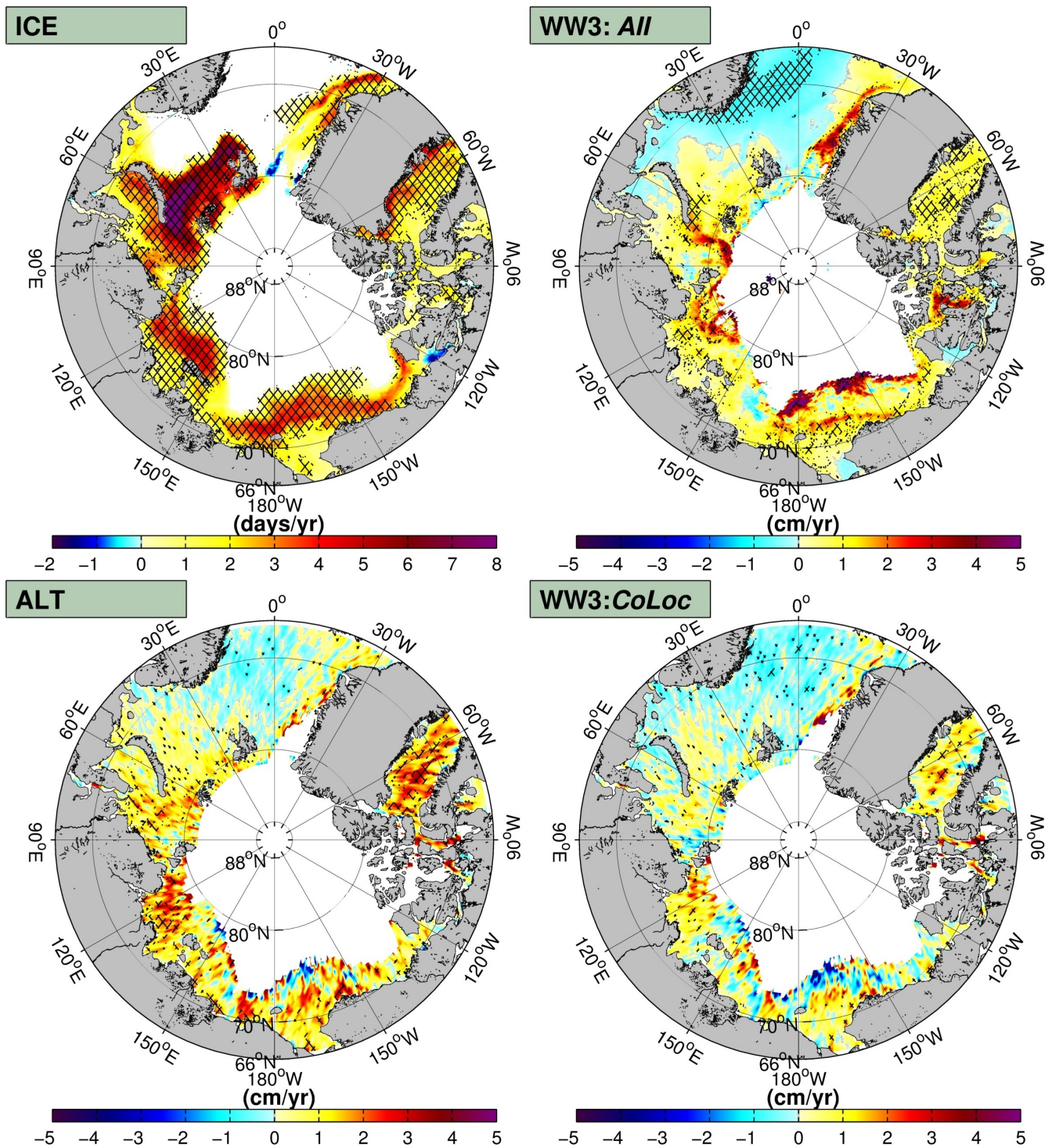


Figure 7. Ice coverage and H_s trends given by Sen's slope with the Mann-Kendall test (thatched-areas) for yearly counts. The top left panel displays the trend of ice-free the annual number of ice-free days per year (ICE) (upper-left panel) and. The other panels show the trends of monthly averaged significant waves from H_s datasets: using the entire wave-dataset (All) 3-hour hindcast (upper-top right panel: All), altimeters (ALT) (lower-bottom left panel: ALT), and co-located wave-model hindcast (lower-bottom right panel: CoLoc) given in terms of day-cm per/year.

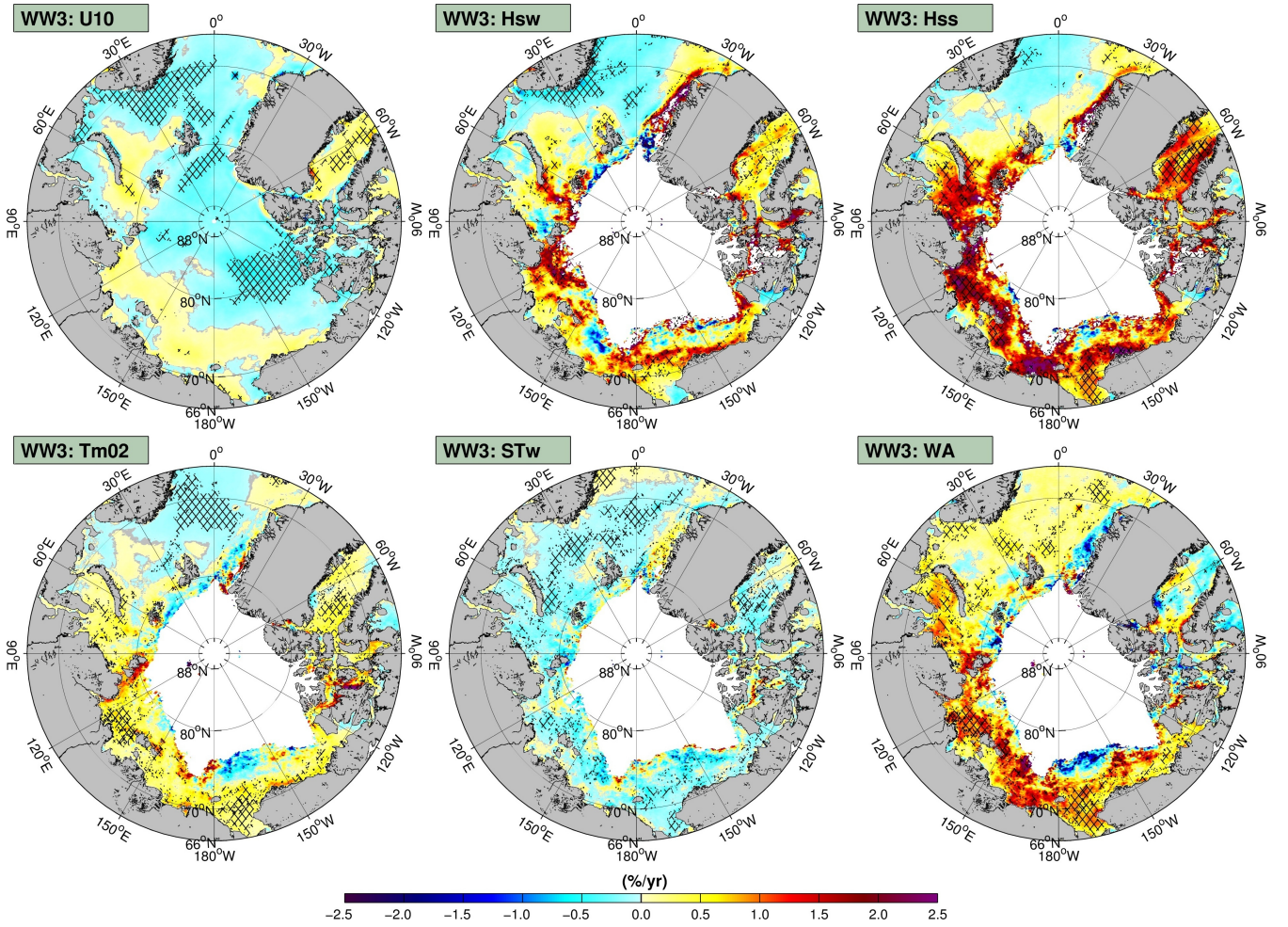


Figure 8. Sen's slope with the Mann-Kendall test (thatched-areas) for monthly averaged wind speeds (U10) (top left panel), wind-sea wave heights (H_{sw}) (top middle panel), swell wave heights (H_{ss}) (top right panel), average wave period (T_{m02}) (bottom left panel), wind-sea steepness (ST_w) (bottom middle panel), and wave age (WA) (bottom right panel) from the wave model-given hindcast in terms of percentage per year relative to the average.

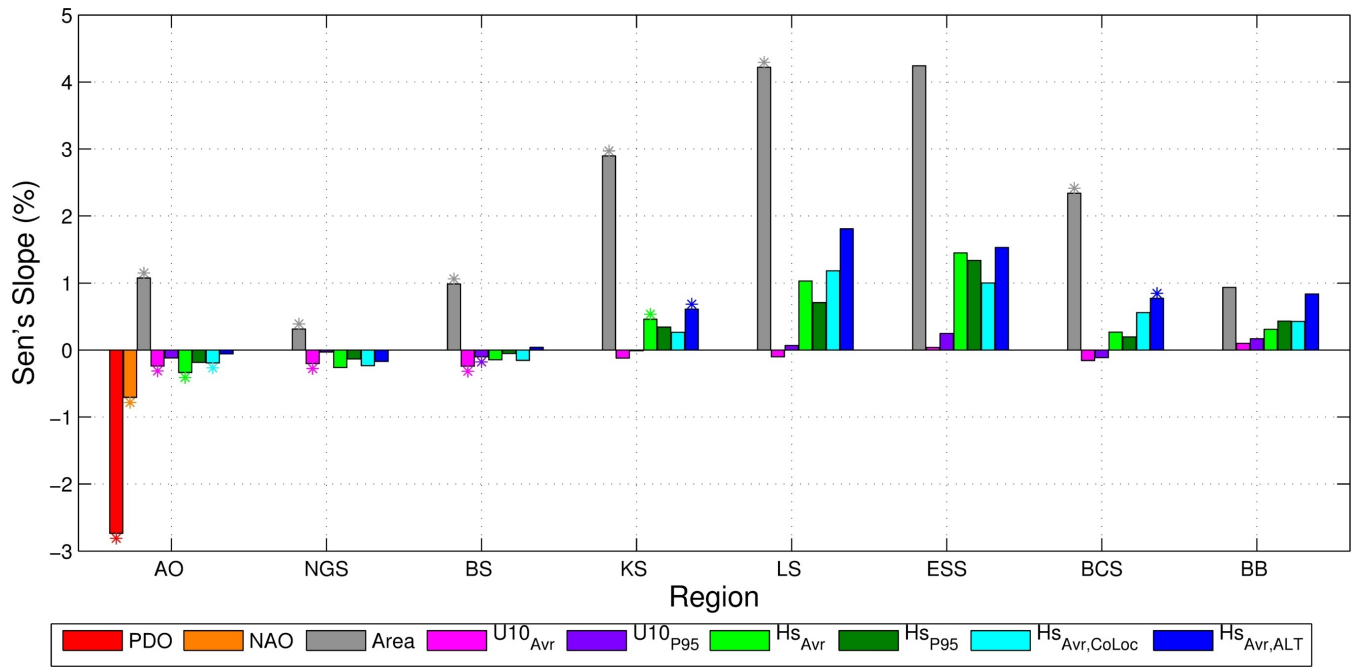


Figure 9. Sen's slope with the Mann-Kendall test (denoted by a '*') for the Arctic Regions of the Arctic Ocean (AO), Nordic-Greenland Sea (NGS), Barents Sea (BS), Kara Sea (KS), Laptev Sea (LS), East Siberia Sea (ESS), Beaufort-Chukchi Sea (BCS), and the Baffin Bay (BB) from monthly time series of the North Atlantic oscillation (NAO), Pacific Decadal Oscillation (PDO), ocean area (Area), wind speed (U10), significant wave heights ~~using all from the 3 hour~~ model data (H_{sAvr} and H_{sP50} H_{sP95}), ~~significant wave heights using and~~ co-located model and altimeter data ($H_{sAvr,CoLoc}$, $H_{sAvr,ALT}$).

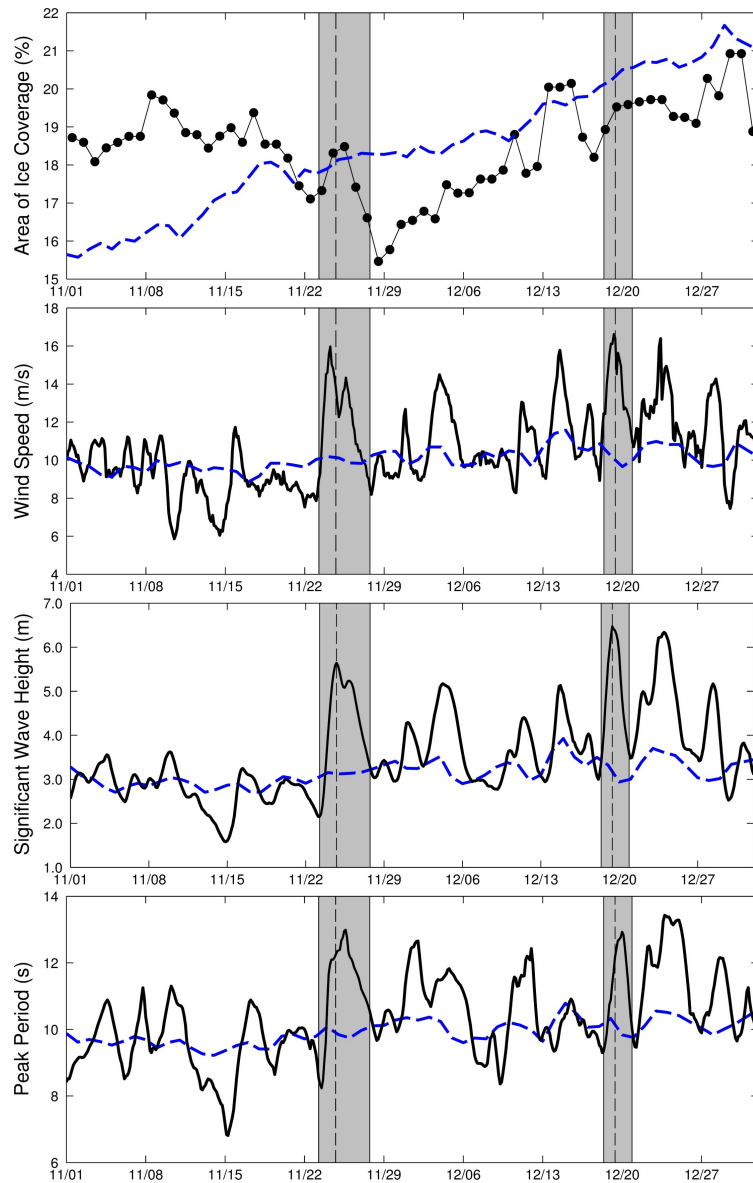


Figure 10. Area-averaged ~~time series of~~ ice coverage, wind speed, significant wave height, and peak period in the ~~Nordic-Greenland~~ Greenland Sea for November-December 1992 (solid line). The dashed line is the daily average from 1992-2014.

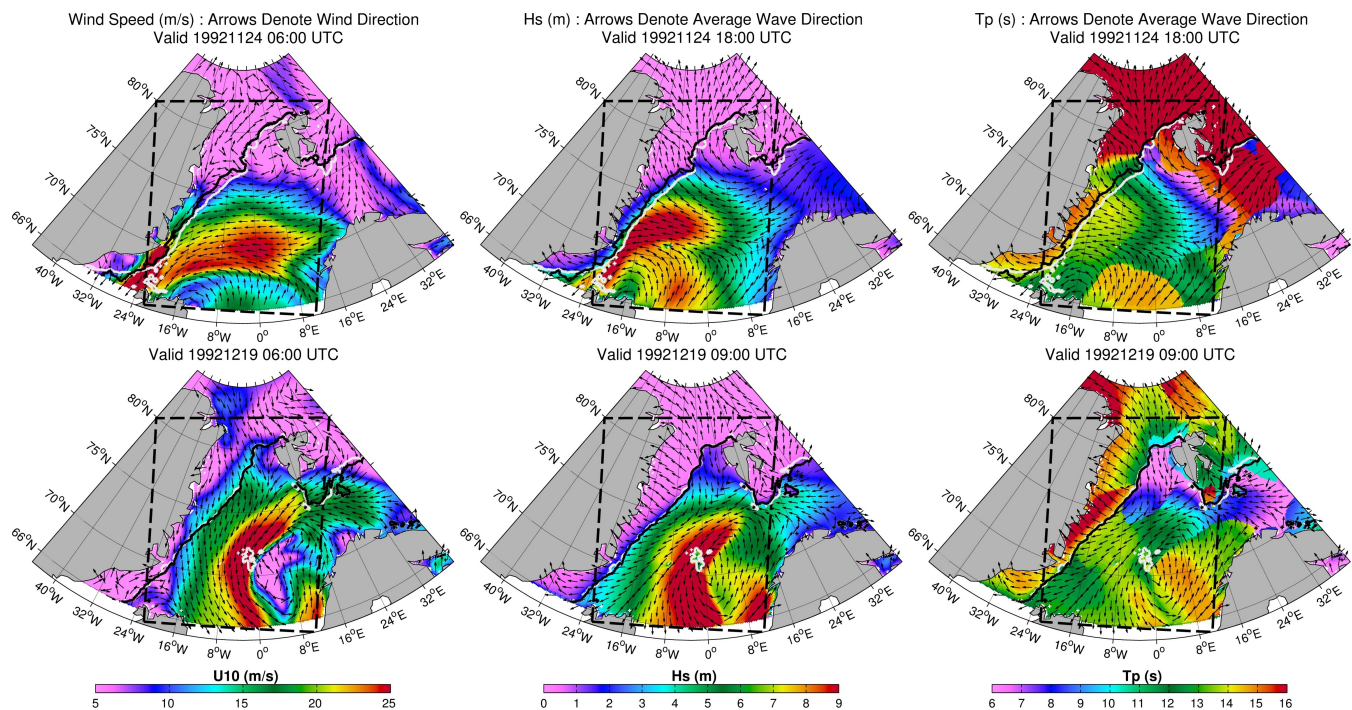


Figure 11. Wind speeds, significant wave heights, and peak periods for ~~two selected~~ events in November and December 1992. The arrows denote ~~either~~ the wind direction or average wave direction. The ~~white and black~~ contour lines represent the ~~ice edge defined by a 15%~~ ice concentration before (white) and after (black) the event.

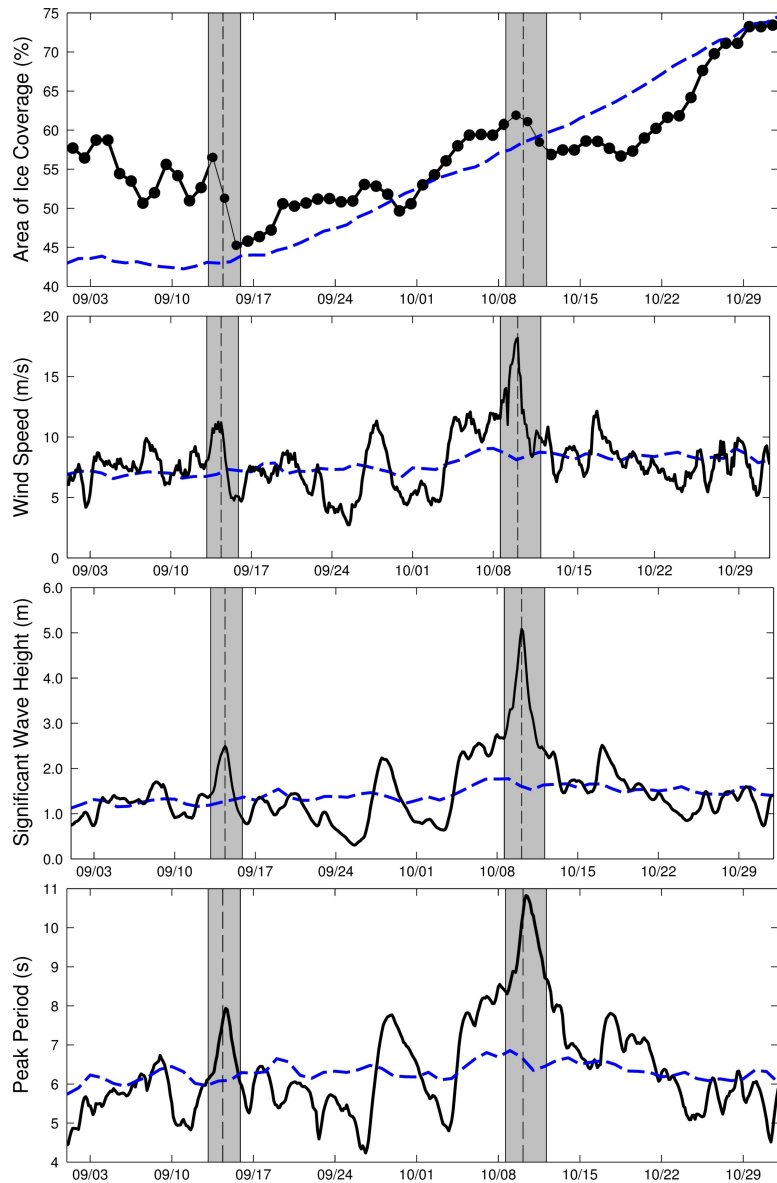


Figure 12. Area-averaged ~~time-series of~~ ice coverage, wind speed, significant wave height, and peak period in the Beaufort-Chukchi Sea for September-October 2006 (solid line). The dashed line is the daily average from 1992-2014.

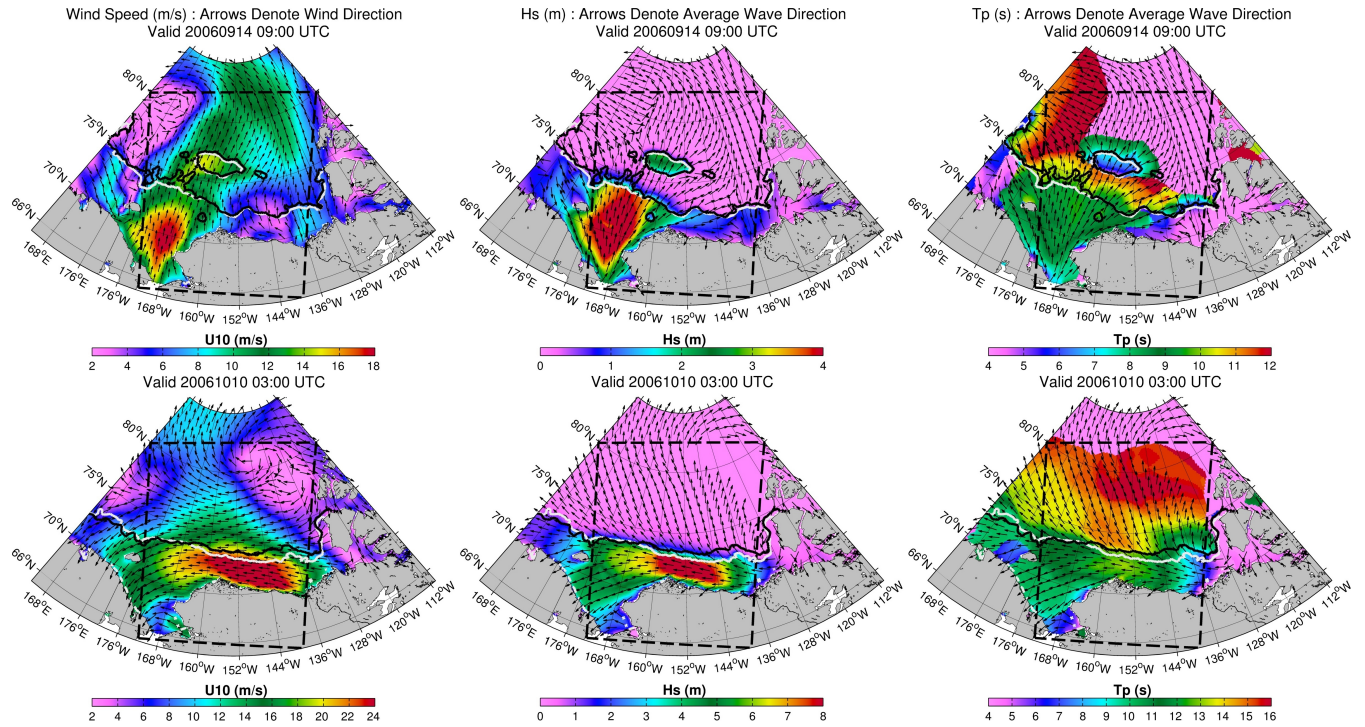


Figure 13. Wind speeds, significant wave heights, and peak periods for ~~two selected~~ events in September and October 2006. The arrows denote ~~either~~ the wind direction or average wave direction. The ~~white and black~~ contour lines represent the ~~ice edge defined by a 15% ice~~ concentration before (white) and after (black) the event.

Table A1. H_s error metrics for select years in the Beaufort-Chukchi Sea using CFSR and ERAI in parentheses.

Buoy ID	Depth (m)	Years Valid (YY)	N	NBIAS (%)	RMSE (m)	SI (%)	R	NSTD (%)
All	-	12,13,14	7574	+8.44 (-3.14)	0.29 (0.25)	20.71 (20.05)	0.94 (0.94)	+1.42 (-5.55)
WMO48213	50.01	13	1700	+11.40 (+1.36)	0.31 (0.28)	25.99 (26.39)	0.91 (0.91)	+6.22 (+6.97)
WMO48214	36.13	12,13,14	3956	+7.79 (-3.52)	0.27 (0.24)	17.55 (16.43)	0.94 (0.95)	+0.79 (-9.06)
WMO48213	41.16	12	568	+5.66 (-3.67)	0.28 (0.23)	15.68 (13.57)	0.95 (0.95)	-11.66 (-10.30)
WMO48211	32.52	13	1350	+9.95 (-8.22)	0.30 (0.26)	30.72 (27.53)	0.87 (0.88)	+10.61 (-13.24)

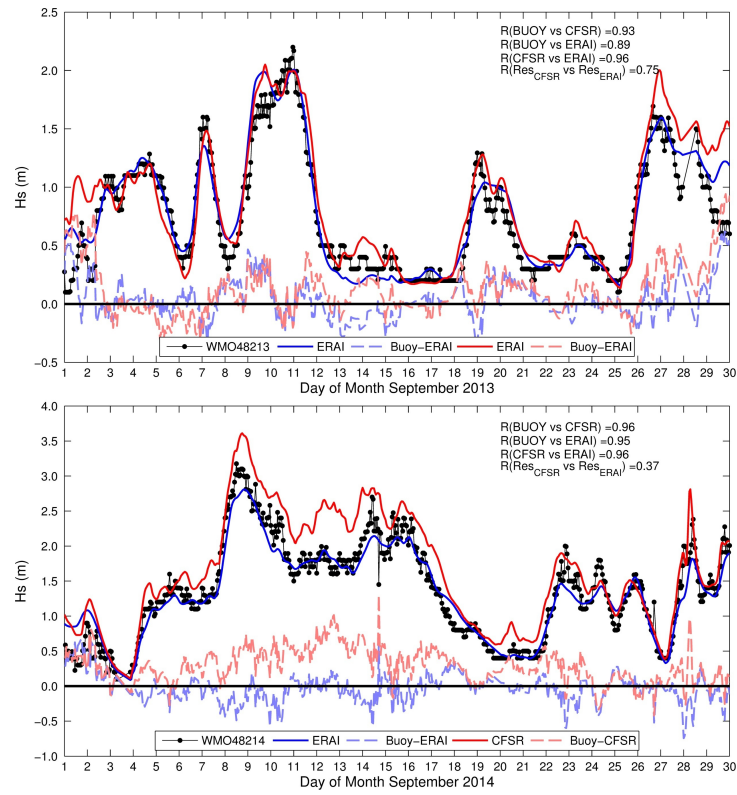


Figure A1. Buoy H_s time series for September 2013 (top) and 2014 (bottom). The solid red and blue lines denotes ERAI and CFSR. The dashed lines represent the residual (buoy-model).

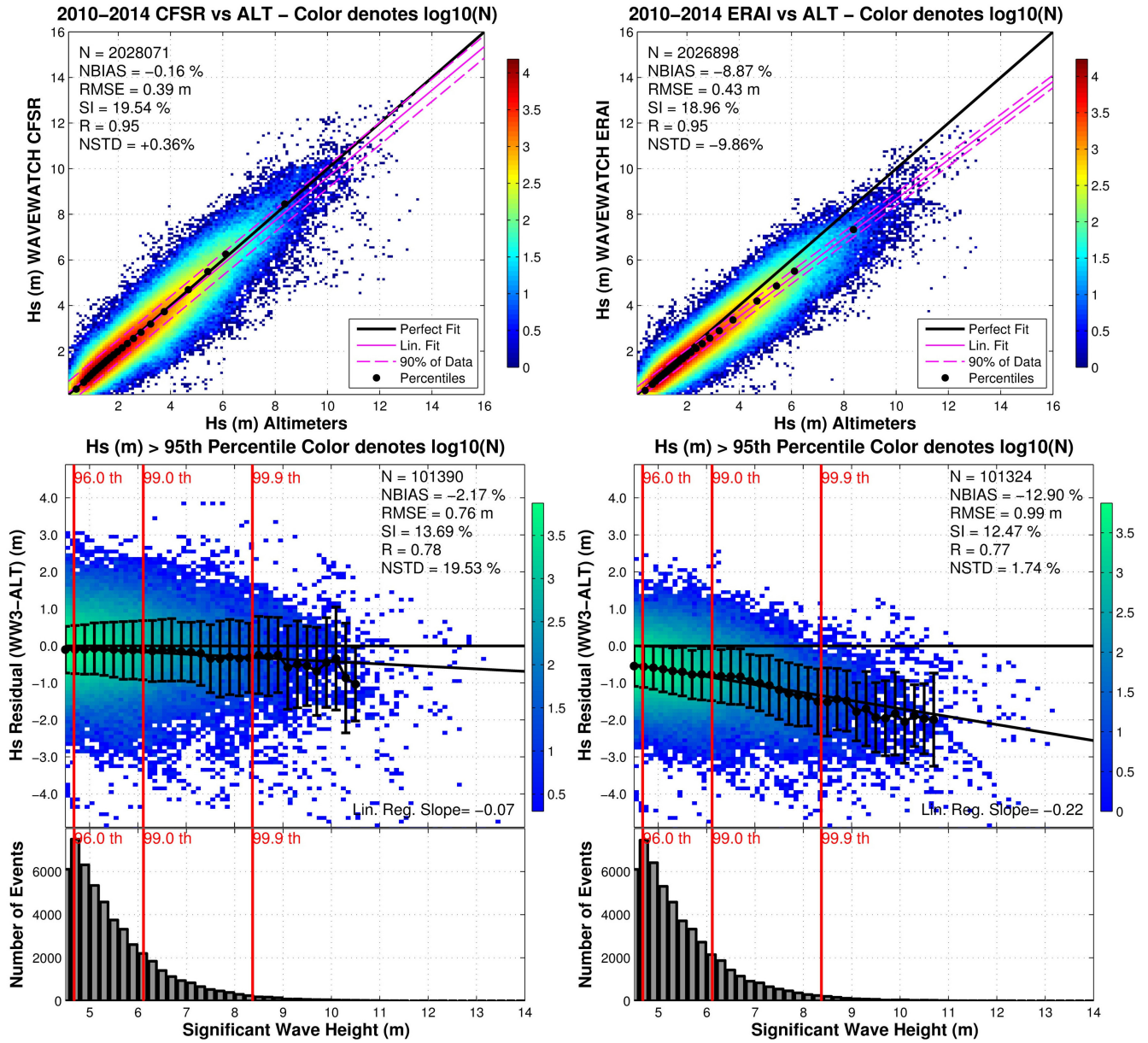


Figure A2. Significant wave height comparison from CFSR (left) and ERAI (right) versus co-located data from altimeters. The error dispersion of the models is presented in a scatterplot with the density given in a logarithmic scale (top panels). The upper percentiles are highlighted to show the differences (bottom panels).

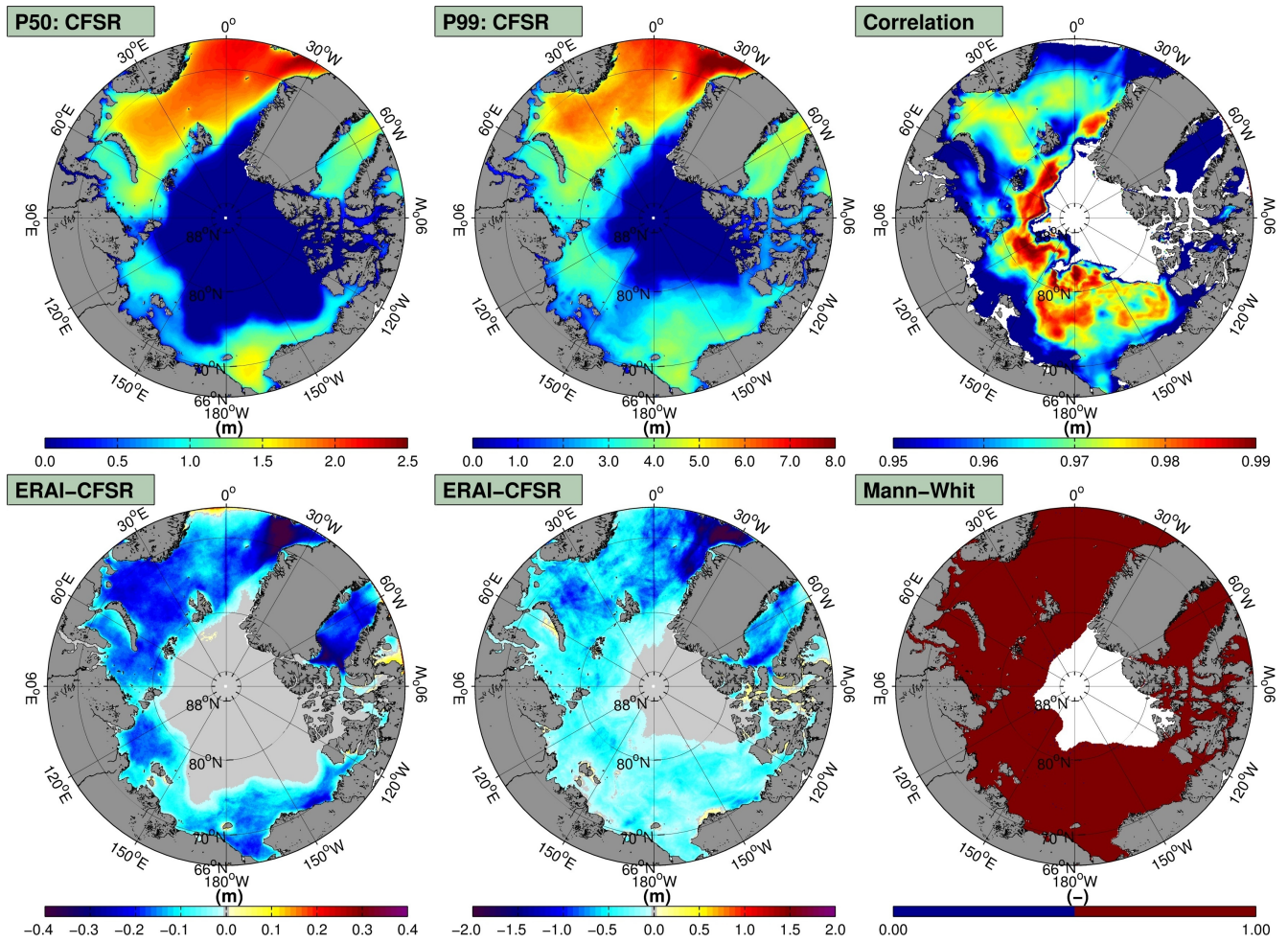


Figure A3. The 50th and 99th H_s CFSR percentiles (2010-2014) (top left and middle panels). ERAI-CFSR 50th and 99th percentiles are given in the bottom left and middle panels. The top right panel shows the correlation coefficients between ERAI and CFSR for a monthly averaged time series between CFSR and ERAI. The Mann-Whitney test is presented in the bottom right panel at the 99.9 % confidence limit.

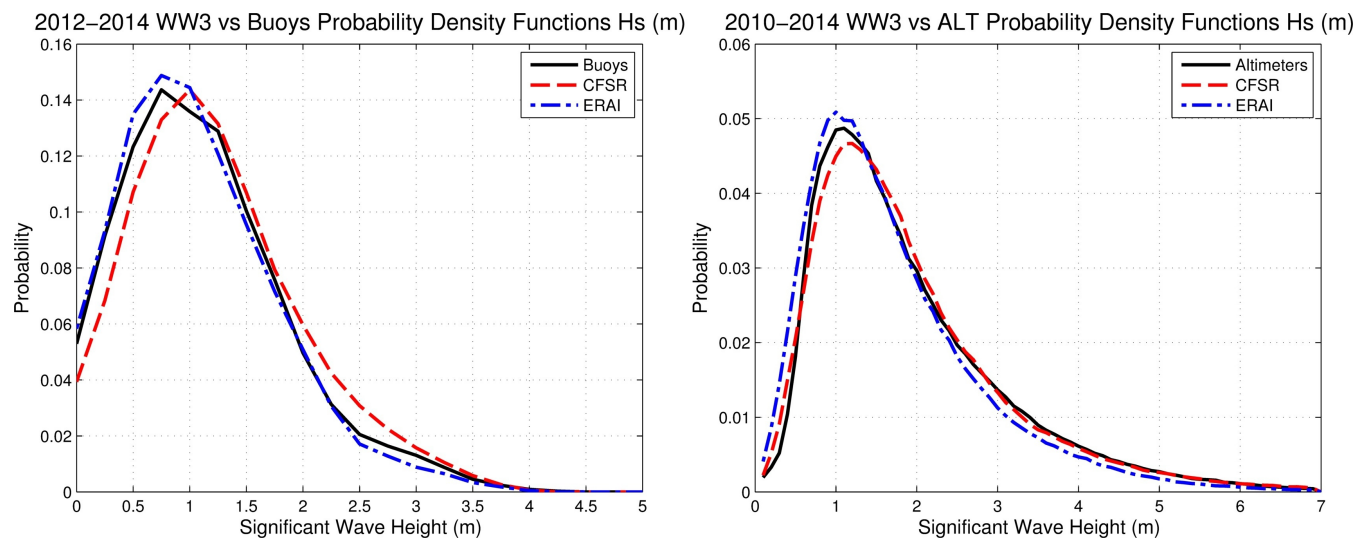


Figure A4. H_s probability distributions for CFSR and ERAI versus the buoys (left) and altimeters (right).

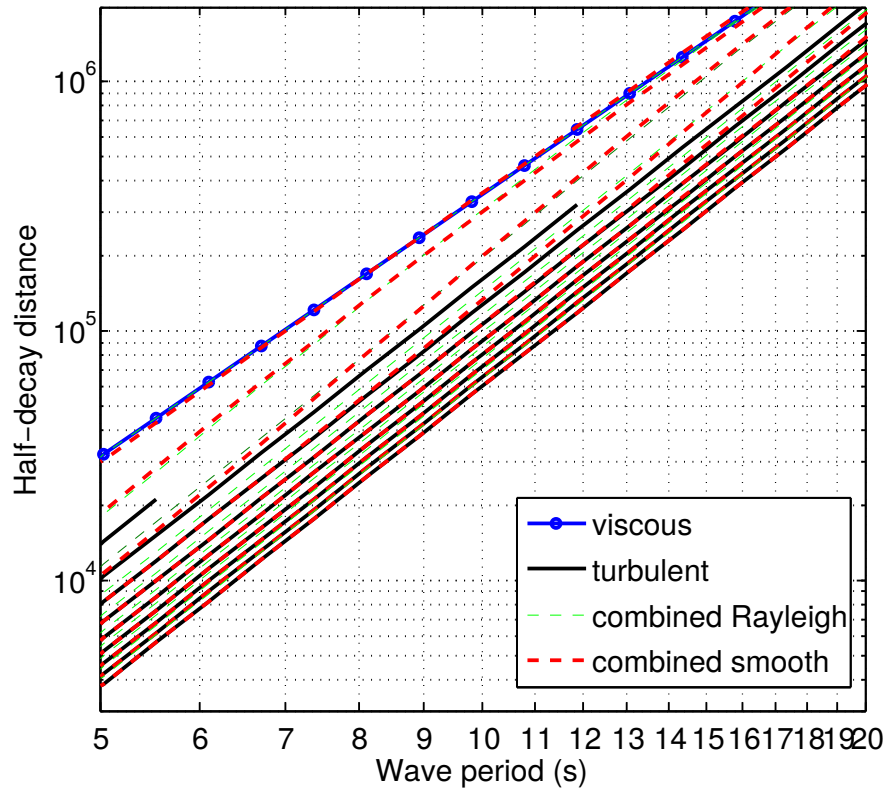


Figure B1. Half-decay distances as a function of the wave period T , and the significant wave height H_s . H_s is varied from 0.5 (upper curves) to 5 m (lower curves). The combination of viscous and turbulent expressions is made using either a Rayleigh distribution of wave height and computing the dissipation for each wave height in the distribution, or by a smooth linear combination of the viscous and turbulent terms adjusted to reproduce the Rayleigh result.

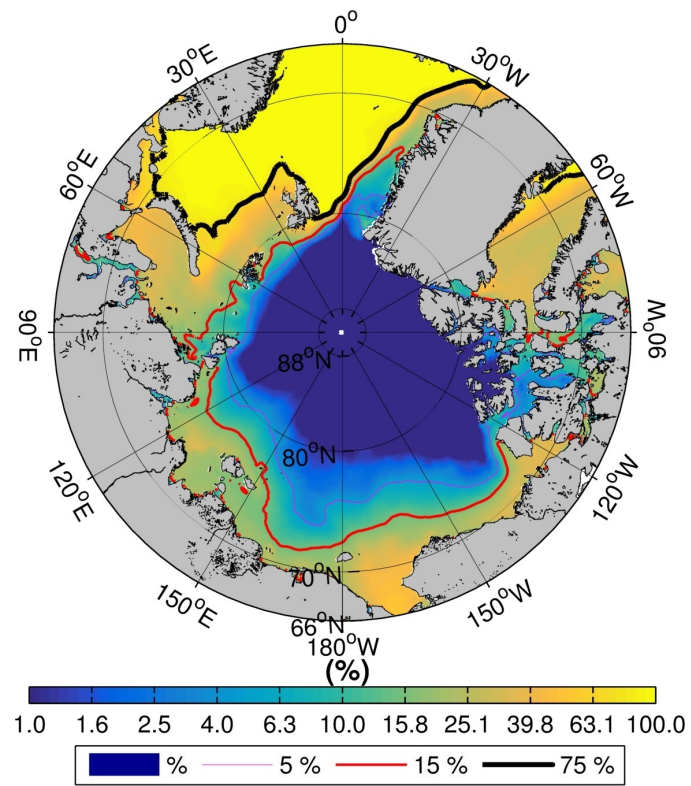


Figure C1. Percentage of ice-free time. Contours represent the 5 (thin purple line), 15 (medium red line), and 75 (thick black line).

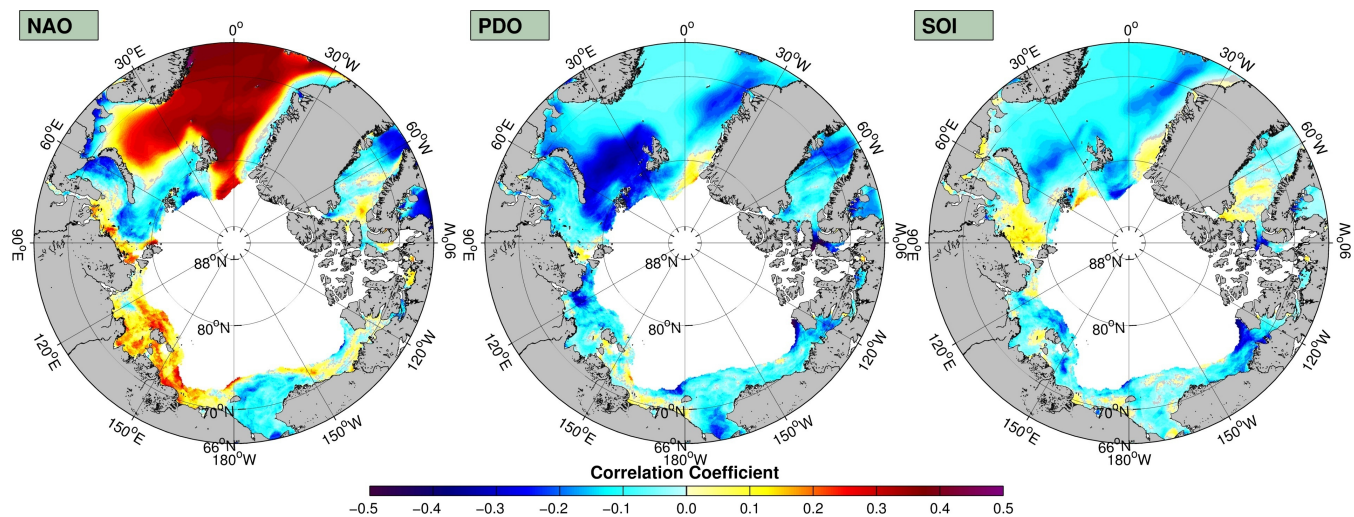


Figure D1. Correlation coefficients calculated from monthly time series of H_s of CFSR and the North Atlantic Oscillation (left) and Pacific Decadal Oscillation (right).